Why Zinc Fingers Prefer Zinc: Ligand-Field Symmetry and the Hidden Thermodynamics of Metal Ion Selectivity[†,‡]

Marcel J. Lachenmann,[§] John E. Ladbury,[||] Jian Dong, Kun Huang, Paul Carey, and Michael A. Weiss*

Department of Biochemistry, Case Western Reserve University, 10900 Euclid Avenue, Cleveland, Ohio 44106-4935

Received April 21, 2004; Revised Manuscript Received August 9, 2004

ABSTRACT: The zinc finger, a motif of protein−nucleic acid recognition broadly conserved among eukaryotes, is a globular minidomain containing a tetrahedral metal-binding site. Preferential coordination of Zn^{2+} (relative to Co^{2+}) is proposed to reflect differences in ligand-field stabilization energies (LFSEs) due to complete or incomplete occupancy of d orbitals. LFSE predicts that the preference for Zn^{2+} should be purely enthalpic in accord with calorimetric studies of a high-affinity consensus peptide (CP-1; Blasie, C. A., and Berg, J. (2002) *Biochemistry 41*, 15068−73). Despite its elegance, the general predominance of LFSE is unclear as (i) the magnitude by which CP-1 prefers Zn^{2+} is greater than that expected and (ii) the analogous metal ion selectivity of a zinc metalloenzyme (carbonic anhydrase) is driven by changes in entropy rather than enthalpy. Because CP-1 was designed to optimize zinc binding, we have investigated the NMR structure and metal ion selectivity of a natural finger of lower stability derived from human tumor-suppressor protein WT1. Raman spectroscopy suggests that the structure of the WT1 domain is unaffected by interchange of Zn^{2+} and Co^{2+}. As in CP-1, preferential binding of Zn^{2+} (relative to Co^{2+}) is driven predominantly by differences in enthalpy, but in this case the enthalpic advantage is less than that predicted by LFSE. A theoretical framework is presented to define the relationship between LFSE and other thermodynamic factors, such as metal ion electroaffinities, enthalpies of hydration, and the topography of the underlying folding landscape. The contribution of environmental coupling to entropy−enthalpy compensation is delineated in a formal thermodynamic cycle. Together, these considerations indicate that LFSE provides an important but incomplete description of the stringency and thermodynamic origin of metal-ion selectivity.

Tetrahedral coordination of Zn^{2+} is ubiquitous among metalloproteins wherein the bound metal ion may play a structural or catalytic role (*1*). Such modules, exemplified by classical Zn fingers and nuclear hormone receptors (*2*−*4*; Figure 1), are ubiquitous among eukaryotic transcription factors and play essential roles in cell-type-specific regulation of gene expression (*5*). Single fingers exhibit metal-dependent folding (*6*) as minidomains (*7*, *8*) similar in structure to corresponding elements of protein−DNA complexes (Figure 1A; *3*). Metal ion coordination is effected by side chains of cysteine and histidine (consensus sequence (F/Y)-X-*C*$X_{2,4}$-*C*-X_3-F-X_5-L-X_2-*H*-X_{3-5}-*H*; ligands in italics). Why do such proteins prefer Zn^{2+} to Co^{2+} (*9*, *10*)? In the present study we investigate an important and general hypothesis regarding the physical origins of metal ion selectivity of tetrahedral Zn^{2+}-binding sites in proteins: that preference for Zn^{2+} relative to Co^{2+} reflects *ligand-field stabilization energies* (LFSEs;[1] *9*), a fundamental feature of crystal-field theory (*11*). Our approach focuses on the thermodynamic signature of LFSE—absence of entropy-enthalpy compensation (EEC)—and considers the relationship between LFSE and other determinants of stability. An experimental model is provided by a Zn finger derived from human tumor-suppressor protein WT1 (*12*, *13*).

The essence of LFSE is as follows. Binding of a metal ion is accompanied by its dehydration and transition from an octahedral environment in solution to a tetrahedral environment in the protein-binding site. In the case of an incomplete d electronic shell (such as that of Co^{2+}), this transition leads in principle to a thermodynamic penalty due to LFSE (Figure 2A; *9*). This penalty arises from differences in the crystal-field splitting of d-orbital energy levels in an

[†] J.E.L. is a Wellcome Trust Senior Research Fellow. This work was supported in part by the Cleveland Center for Structural Biology and by a grant from the National Institutes of Health to M.A.W. (R01 CA 063485).

[‡] Coordinates and restraints have been deposited in the Protein Data Bank as entry 1XF7.

* To whom correspondence should be addressed. E-mail: michael.weiss@case.edu. Phone: (216) 368-5991. Fax: (216) 368-3419.

[§] Present address: Harvard Medical School, Boston, MA 02115.

[||] Present address: Department of Biochemistry and Molecular Biology, University College London, Gower St., London WC1E 6BT, England.

[1] Abbreviations: CAII, carbonic anhydrase II; DG, distance geometry; EEC, entropy−enthalpy compensation; ITC, isothermal titration calorimetry; LFSE, ligand-field stabilization energy; NMR, nuclear magnetic resonance; NOE, nuclear Overhauser enhancement; NOESY, NOE spectroscopy; RMD, restrained molecular dynamics; RMS; root-mean-square; RMSD, RMS difference; WT1-p, synthetic peptide derived from finger 3 of human tumor-suppressor protein WT1; 2D, two-dimensional; 3D, three-dimensional. Amino acids are designated by standard single- and three-letter codes. The phrase "hidden thermodynamics" (title and Discussion) is due to Karplus and co-workers (*94*). "Nominal" properties refer to structural and dynamic features of the protein without consideration of solvent (*24*).

10.1021/bi0491999 CCC: $27.50
Published on Web 10/13/2004

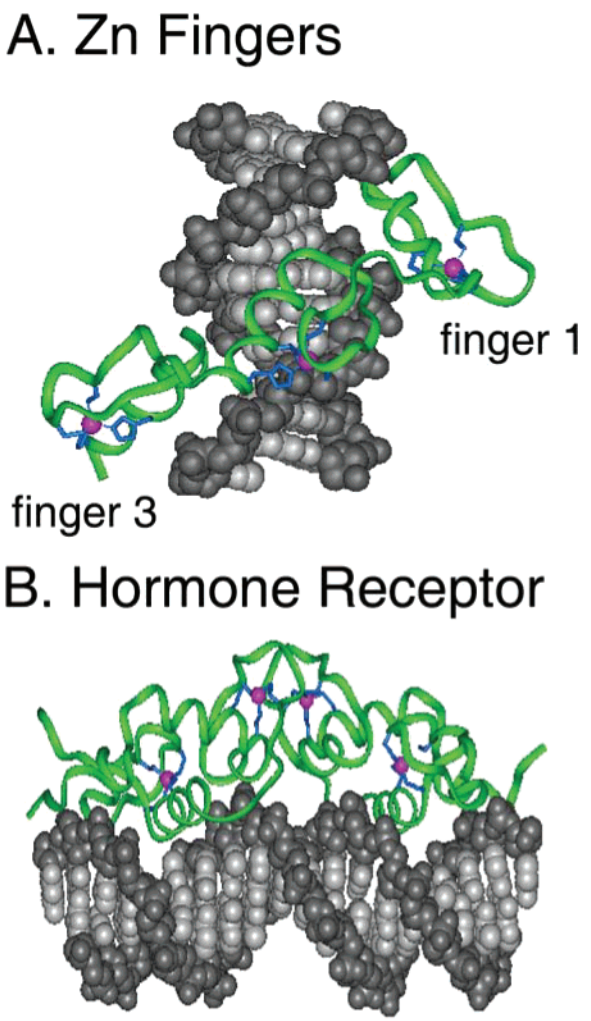

FIGURE 1: Evolution of Zn modules in eukaryotic transcription factors. Crystal structures of (A) Zif268 Zn finger−DNA complex (*3*) and (B) glucocorticoid receptor (GR)−DNA complex (*4*). Increased zinc availability during aerobic transition of the Proterozoic era enabled metal ion-dependent folding of peptide cages. Proteins are depicted as green ribbons and zinc ions as magenta spheres. Protein ligands (Cys and His side chains) are represented as blue sticks. The DNA backbone and bases are shown in dark and light gray, respectively. PDB codes for Zif268−DNA and GR−DNA complexes are 1ZAA and 1GLU, respectively.

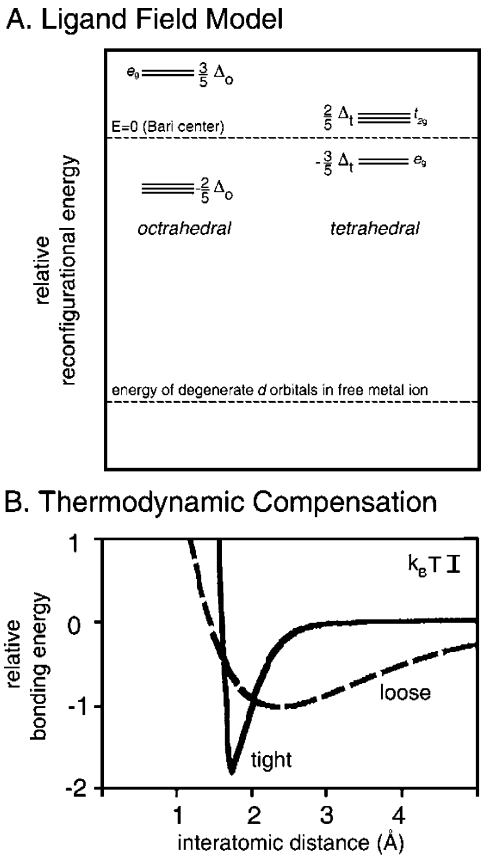

FIGURE 2: Ligand-field stabilization energy and entropy−enthalpy compensation. (A) Crystal-field splitting of d energy levels of d^7 Co^{2+} and d^{10} Zn^{2+} ions in aqueous solution (octahedral environment; left-hand panel) and within the Zn finger (tetrahedral environment; right-hand panel). Dashed lines indicate the mean energy of LFSE-split orbitals (Bari center; upper line) and energy of degenerate d orbitals of free metal ion in the gas phase (lower line). Energy differences (upper and lower groups of orbitals) are designated Δ_o (octahedral) and Δ_t (tetrahedral). The lobes of e_g orbitals ($d_{x^2-y^2}$ and d_{z^2}) point along the *x*, *y*, and *z* axes, whereas the lobes of the t_{2g} orbitals (d_{xy}, d_{xz}, and d_{yz}) point between axes. This figure is adapted from Lippard and Berg (*11*). (B) Gas-phase and environmental models of EEC. Electrostatic potential wells in which tight associations permit little motion whereas weak associations permit significant residual motion within the bound state. A perturbation resulting in a transition from a strong to a weak interaction will result in a loss of enthalpy compensated by a gain in entropy. This panel is adapted from Williams and co-workers (*22*).

octahedral field (left-hand panel of Figure 2A) or a tetrahedral field (right-hand panel of Figure 2A). Whereas the complete d^{10} shell of Zn^{2+} leads to the same average energy in either ligand field (the Bari center; upper dashed line), the d^7 shell of Co^{2+} exhibits an LFSE of $-4/5\Delta_o$ in an octahedral field (relative to the Bari center) and $-6/5\Delta_t$ in a tetrahedral field (where Δ_o and Δ_t are respective d-orbital splittings for octahedral and tetrahedral fields). Because Δ_o is almost twice as large as Δ_t, octahedral coordination should be preferred. On the basis of model compounds, the difference in free energy of binding is predicted to be about −4.5 kcal/mol.[2] In qualitative accord with such reasoning, experimental affinities of finger peptides and other globular metal-binding motifs for Zn^{2+} are 10^2-10^4-fold higher than their affinities for Co^{2+} (*11*).

[2] This estimate was based on studies of the zinc $(S\text{-Cyc})_2(His)_2$ center of bis(2,4,6-triisopropylbenzenethiolate)bis(*N*-methylimidazole)cobalt(II) (*9*, *95*).

LFSE exhibits a characteristic thermodynamic signature: preferential binding of Zn^{2+} (relative to Co^{2+}) is driven by enthalpy without incurring entropic compensation. Absence of EEC, as observed in calorimetric studies of a consensus Zn finger (CP-1; *14*), is striking as the binding of metal ions to organic cages and globular proteins is ordinarily complex (*15*−*18*): distinction between enthalpic and entropic driving forces is generally confounded by EEC. EEC, observed in a wide range of chemical and biochemical processes (*19*, *20*), is often ascribed to competition between noncovalent bonding and dynamics, which engenders a tradeoff between favorable interactions (ΔH) and unfavorable immobilization (ΔS) within "tight" and "loose" potential wells (Figure 2B; *21*, *22*). Compensation may also be mediated by solvent reorganization and other forms of environmental coupling (*23*, *24*). Almost complete solvent-mediated compensation, for example, underlies the lack of significant metal ion selectivity

Table 1: Dissociation Constants for Co^2 and Zn^2 for Diverse Metalloproteins

protein/domain	K_d (Co^{2+}) (M)	K_d (Zn^{2+}) (M)	ratio	pH	ref
		A. Classical Fingers			
TFIIIA	$(3.8 \pm 0.5) \times 10^{-6}$	$(2.8 \pm 0.9) \times 10^{-9}$	1400	7.0	*9*
CP-1	$(6.3 \pm 2.2) \times 10^{-8}$	$(5.7 \pm 1.3) \times 10^{-12}$	11000	7.0	*82*
CP-CCHC	$(6.3 \pm 2.2) \times 10^{-8}$	$(3.2 \pm 1.0) \times 10^{-12}$	20000	7.0	*82*
CP-CCCC	$(3.5 \pm 1.0) \times 10^{-7}$	$(1.1 \pm 0.3) \times 10^{-12}$	32000	7.0	*82*
		B. Nonclassical Fingers			
RMLV	1×10^{-6}	6×10^{-10}	1700	7.0	*83*
HIV-CCHC	9.0×10^{-8}	7.0×10^{-11}	1300	7.0−8.0	*84*−*86*[a]
NZF-1	$(4 \pm 2) \times 10^{-7}$	$(1.4 \pm 0.8) \times 10^{-10}$	2900	6.9	*87*
		C. Globular Proteins			
CAII	$(2 \pm 1.4) \times 10^{-8}$	$(8.3 \pm 1) \times 10^{-13}$	24000	7.0	17

[a] Values were summarized by Godwin and colleagues (85) from refs 84−86.

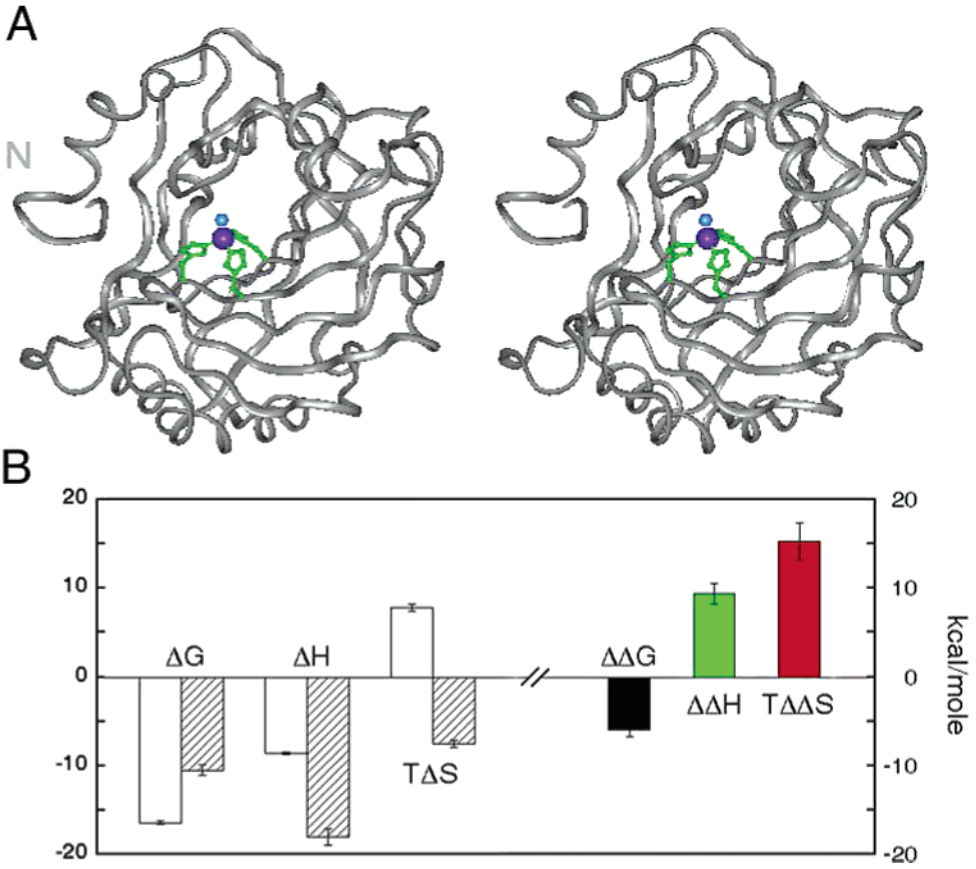

FIGURE 3: Structure and thermodynamic studies of carbonic anhydrase II. (A) Ribbon model of CAII and active-site Zn^{2+} ion (purple), (stereo representation). Also shown are inner-shell protein ligands (residues H94, H96, and H119; green) and bound hydroxide ion (blue). Coordinates were obtained from the Protein Data Bank (accession code 1CA2; *54*). Crystal structures of the Zn^{2+} and Co^{2+} metalloenzymes are essentially identical (PDB accession code 1CAH; *68*). (B) Histogram showing the results of ITC analysis. Open bars at the left pertain to binding of Zn^{2+}; hatched bars pertain to binding of Co^{2+}. Thermodynamic double differences are shown at the right: $\Delta\Delta G$ (black), $\Delta\Delta H$ (green), and $T\Delta\Delta S$ (red). A large value of $T\Delta\Delta S$ is inconsistent with the LFSE model.

of derivatives of ethylenediaminetetraacetic acid (*15*). Solvent-mediated EEC likewise underlies the maintenance of native zinc affinity by a Zn finger variant (*25*, *26*).

Our interest in the generality of LFSE is motivated by two apparent inconsistencies. First, whereas LFSE predicts a single universal factor by which Zn fingers prefer Zn^{2+} to Co^{2+}, a broad range of binding ratios (and hence of $\Delta\Delta G$ values) is observed (Table 1). The enthalpic advantage observed in the binding of Zn^{2+} to consensus finger CP-1 ($\Delta\Delta H$ = ca. 7−8 kcal/mol relative to Co^{2+}; *14*), for example, significantly exceeds the expected LFSE contribution (4.5 kcal/mol; *9*). Second, whereas LFSE should apply not only to Zn fingers but also to classical tetrahedral Zn-binding sites in metalloenzymes, a recent thermodynamic analysis of carbonic anhydrase II (CAII; Figure 3A)[3] has yielded discrepant results (Figure 3B; *17*). Although as expected the affinity of CAII is greater for Zn^{2+} than Co^{2+} ($\Delta\Delta G° = -5.9$ kcal/mol; black bar at right; *17*, *27*), such selectivity is driven by the difference between *entropic* changes ($T\Delta\Delta S° = 15.3$

[3] This ubiquitous metalloenzyme catalyzes the reversible hydration of carbon dioxide to bicarbonate (*96*). The structure of CAII is well characterized by X-ray crystallography as both Zn^{2+} and Co^{2+} complexes (*54*, *65*, *67*, *68*). These high-resolution structures are essentially identical (*65*−*67*).

kcal/mol; red bar) with incomplete enthalpic compensation (green bar). Although this apparent breakdown of the LFSE model is not well understood, Toone and colleagues have suggested that the more favorable enthalpy of Co^{2+} binding (ΔH; shaded bar in the left-hand panel of Figure 3B) reflects differences between respective enthalpies of hydration (*17*).[4] Although germane to the general dehydration step of metal ion binding, how enthalpies of hydration relate to LFSE is not apparent. Indeed, despite their individual claims of generality, these perspectives make opposite thermodynamic predictions.

In this study we investigate the hidden thermodynamics of metal ion selectivity and consider its theoretical foundations. To extend the study of a consensus Zn finger of optimal design (*14*), a natural finger of lower thermodynamic and dynamic stability is employed. A model is provided by a peptide (designated WT1-p) derived from WT1 (*12*), a tumor-suppressor protein associated with Wilms' tumor and required for development of the kidney and genitourinary system (*13*, *28*). The high-resolution structure of the WT1-p Zn finger is determined by homonuclear 3D NMR spectroscopy (*29*), and its similarity to the corresponding Co finger demonstrated by Raman spectroscopy (*30*). Remarkably, as in CP-1 (*14*), preference of the Zn finger for Zn^{2+} circumvents EEC (i.e., $\Delta\Delta G$ is predominantly enthalpic), but in WT1 the magnitude of $\Delta\Delta H$ (3.3 ± 0.7 kcal/mol) is less than expected on the basis of LFSE. Given the universality of crystal-field theory and the structural homology between CP-1 and WT1, why are such marked deviations in $\Delta\Delta H$ (and hence in the stringency of metal ion selectivity) observed? A general thermodynamic analysis is proposed to clarify the limitations of the LFSE viewpoint and its relationship to other thermodynamic contributions, including respective enthalpies of metal ion hydration (*17*) and intrinsic electroaffinities (the Irving−Williams series; *10*, *31*). Because of the differences between CP-1 and WT1 in stability and dynamics, a general coupling is envisaged between metal ion selectivity and the topography of the underlying energy landscape (*32*, *33*). An essential distinction is proposed between "open" and "closed" metal-binding sites that provides a microscopic view of thermodynamic compensation (*34*).

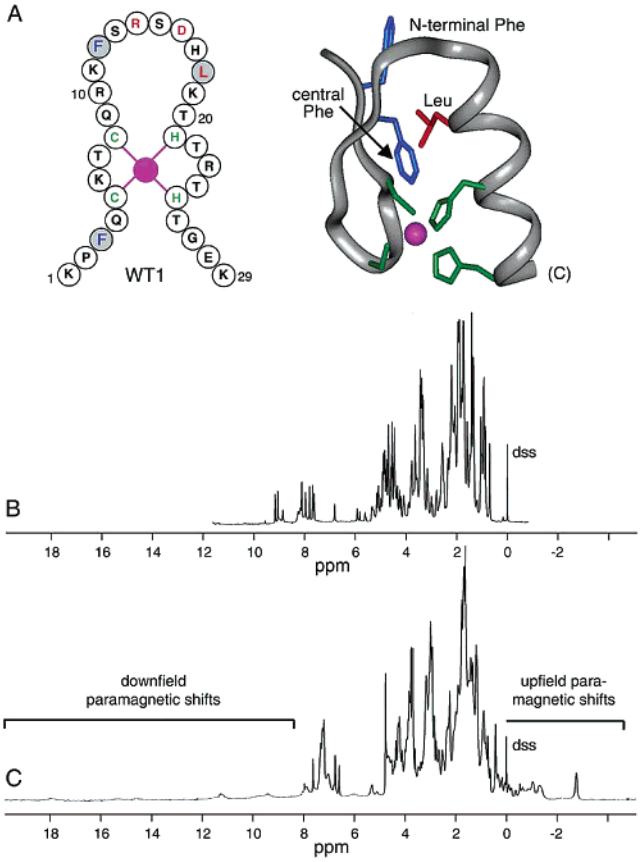

FIGURE 4: WT1-p and NMR spectra of its Zn^{2+}- and Co^{2+}-peptide complexes. (A) Left: peptide sequence of WT1-p. Cysteate and histidine ligands are shown in green, and the metal ion is shown in magenta. Framework hydrophobic residues are shaded; the solvent-exposed Arg-Asp DNA recognition element is in red. The numbering scheme refers to the synthetic peptide (29 residues). Right: ribbon model of the Zn finger showing Zn^{2+} (magenta), ligands (two cysteate and two histidine side chains; green), conserved leucine (red), and the consensus aromatic side chain (green). The C-terminus of the peptide is indicated as "(C)". (B, C) Comparison of 1D ^{1}H NMR spectra of the Zn^{2+}-bound peptide (B) and Co^{2+}-bound peptide (C). Spectra were observed at 25 °C in D_2O in 10 mM deuterated Tris−DCl (pH 7.0) and 140 mM KCl. Chemical shifts are referenced to the proton resonance of 5,5′-dimethylsilapentanesulfate (dss), assumed to be at 0 ppm.

MATERIALS AND METHODS

Peptide Synthesis. The sequence of the WT1-p (Figure 4A) is derived from finger 3 of human WT1. The peptide was obtained by solid-phase synthesis (*35*) as described (*25*).

Isothermal Titration Calorimetry. Data were obtained using an Omega ITC or MCS ITC, both from Microcal, Inc. (Northampton, MA), as described (*25*). Titrations were performed at 25 °C in a buffer solution (50 mM HEPES−HCl at pH 6.5). Precautions were taken to ensure that the Cys residues in the finger remained reduced throughout the ITC experiments. The peptide was dialyzed in a buffer that had been saturated with argon gas to displace dissolved O_2. Titrations were performed immediately after dialysis under airtight conditions. Despite the small diameter of the ITC fill tube (ca. 2 mm) and the seal between the syringe and the cell mountings being almost airtight, the opening was sealed during calorimeter equilibration with Parafilm. A flow of N_2 gas was applied across the cell mounting throughout the experiment to reduce exposure to air. Data were fitted as described (*36*, *37*) after subtraction of respective heats of dissolution of salt into buffer and buffer into peptide solution as obtained in separate control experiments. Results represent the mean of two individual titrations. The overall thermodynamics of metal binding, as measured by ITC, will reflect the net effects of coupled nominal and environmental reactions. Differences between observed ITC values are ascribed to the process of metal-dependent peptide folding. The nominal association reaction is accompanied by transfer of water molecules from the hydration shell of the metal to bulk solvent and changes in solvent reorganization associated with peptide folding. Contributions from metal-dependent peptide folding, solvent reorganization, and buffer ionization presumably cancel in double-difference values ($\Delta\Delta G$, $\Delta\Delta H$, and $T\Delta\Delta S$).

[4] Standard enthalpies of hydration of ions refer to formal transfer of an ion from the gas phase to an infinitely dilute solution. Values are relative to a zero point defined for the reaction H^+ (gas) → H^+ (aqueous) (*97*).

Laser Raman Spectroscopy. Raman studies were determined using a high-light-grasp spectrograph based on a Holospec *f*/1.4 (Kaiser Optical) as described (*38*). Typical conditions were 752 nm, 1 W excitation, and 5 min data collection time. An excitation frequency of 752 nm (Kr^+) was used since 647.1 nm gave rise to unacceptably high light-background levels. The concentration of peptide was 2 mM in 10 mM Tris−HCl (pH 7.5) and 140 mM KCl; the molar ratio of metal ion to peptide in the solution was 1.1:1. The sample volume was 50 μL. The buffer spectrum with the water-bending mode at 1645 cm^{-1} was subtracted from each amide I profile. Since the water band is a broad feature, the subtraction can be carried out with facility and accuracy. Each spectrum was acquired after 5 min of data accumulation.

NMR Spectroscopy. Peptide WT1-p was dissolved in 0.7 mL of NMR buffer containing 50 mM deuterated Tris−HCl (pH 6.1) and 5 mM $ZnCl_2$. 2D experiments were performed as described (*25*). Spectra and assignments are provided in the Supporting Information. NOE and *J*-coupling (dihedral angle) restraints were used for molecular modeling as previously described (*39*). The 2D NOESY experiment was acquired with 4096 complex points and 300 t_1 values. The sweep width was 6500 Hz in both dimensions. NOESY mixing times were 75, 100, and 200 ms. Spectra in H_2O were acquired following selective excitation using shaped pulses as described (*40*). 2D NMR data were Fourier transformed using a combination of exponential and shifted sine bell functions in both dimensions and zero-filled to 4K by 4K points. The 3D TOCSY−NOESY experiment was acquired with 512 complex points, 64 t_1 values, and 128 t_2 values. The sweep width was 6000 Hz in all dimensions. The NOESY mixing time was 200 ms, and the TOCSY mixing time was 40 ms. Data were processed with forward linear prediction to double the number of points in all dimensions, and a combination of exponential and shifted sine bell functions were applied in all dimensions. The data were zero-filled to a final size of 1024 × 512 × 512; first-order drift correction was applied to ω_3.

Molecular Modeling. The volume and location of inferred protein cavities and crevices were obtained using the program SURFNET (*41*). Analysis of polar and nonpolar protein surfaces was obtained using the Connally surface feature implemented in InsightII (Biosym, Inc., San Diego, CA). Static accessible surface areas were obtained with a probe sphere size of 1.4 Å using the program ACCESS (*42*). RMS deviations (Figure 7B) were calculated by pairwise comparison and not in reference to a common mean structure (which would yield smaller numbers).

RESULTS

Our results are presented in two parts. We first provide a formal description of LFSE in relation to a statistical-mechanical model of ligand exchange. This formalism predicts an absence of EEC and makes explicit the assumptions underlying this prediction. We next establish an experimental model—cancer-associated Zn finger WT1-p—in which this theoretical framework is tested in relation to consensus peptide CP-1 (*14*). The metal ion selectivity of WT1-p is predominantly enthalpic in origin but attenuated relative to CP-1. Although WT1-p is shown to retain a canonical $\beta\beta\alpha$ structure (*7*, *8*), its thermodynamic and dynamic stabilities are lower than those of CP-1 and so may be more representative of native fingers. Implications for other Zn-binding sites (such as that of CAII) and the role of enthalpies of hydration are considered in the Discussion.

I. Statistical Mechanics of LFSE. The LFSE mechanism predicts that the change in free energy accompanying exchange of metals between Zn^{2+}- and Co^{2+}-bound fingers ($\Delta\Delta G$)

$$s_N'\cdot P_N'\cdot Co^{2+} + s_M\cdot Zn^{2+} \leftrightarrows s_N\cdot P_N\cdot Zn^{2+} + s_M'\cdot Co^{2+} + (s_\Delta)_{bulk} \quad (1)$$

would be purely enthalpic ($\Delta\Delta H \ll 0$) and without entropic compensation; $T\Delta\Delta S$ would be negligible. This prediction assumes that the bound peptide structures P_N and P_N' are similar, that the same number of water molecules s_i and s_i' participate in solvation (i.e., $s_N = s_N'$ and $s_M = s_M'$, so s_Δ is negligible), and that no protons are bound or released by the domain on exchange of metal ions. This intuition may be formally justified as follows. Let the LFSE be denoted ϵ, and suppose that the native Zn finger is characterized by a density of states $\omega(U)$ such that the number of states with an energy in the range from U to $U + \delta U$ (relative to the apopeptide and solvated ion) is $\omega(U)\,\delta U$ (*19*). The configurational component of its partition function Q is then

$$Q = \int_{-\infty}^{+\infty} \omega(U)\, e^{-\beta U}\, dU \quad (2)$$

We assume that the LFSE is not coupled to the manifold of states describing the apopeptide or metal-bound peptide, i.e., that the structure, dynamics, and solvation of Zn^{2+}- and Co^{2+}-bound fingers are similar. With this assumption, the density of states in the Co finger $\omega'(U)$ is related to $\omega(U)$ by an offset, $\omega'(U) = \omega(U-\epsilon)$, so the difference in mean change in energy between fingers is also ϵ (denoted $\Delta\Delta E$ below; two Δ's are used to emphasize that U is defined above relative to the apopeptide and solvated ion, and so is implicitly a difference value). Similarly, the configurational component of the partition function of the Co^{2+}-bound finger is given by

$$Q' = \int_{-\infty}^{+\infty} \omega(U-\epsilon)\, e^{-\beta U}\, dU = e^{-\beta\epsilon} Q \quad (3)$$

where $\beta = 1/k_B T$, k_B is the Boltzman constant, and T is the temperature. This implies that the difference in change of free energy $\Delta\Delta A$ between Zn^{2+}- and Co^{2+}-bound fingers (relative to their common apopeptide) is

$$\Delta\Delta A = -k_B T \ln\left(\frac{Q'}{Q}\right) = \epsilon = \Delta\Delta E \approx \Delta\Delta H \quad (4)$$

where small differences between mean energy differences $\Delta\Delta E$ and enthalpy $\Delta\Delta H$ are neglected. Compensation is not expected because the shift in the manifold of states is global: perturbations in each degree of freedom external to the metal ion are completely correlated.

The above model neglects several factors. Although Zn^{2+} and high-spin Co^{2+} exhibit similar ionic radii and are each borderline as "hard" or "soft" Lewis acids, the two metals

differ in ionization energies, Pauling electronegativity, and standard electrode potential (*43*). Such properties may lead to differences in the strength of the covalent bonds between the protein and the metal ion unrelated to the symmetry of the ligand field (*10*). Indeed, free imidazole and cysteine bind more tightly to Zn^{2+} than to Co^{2+} (*44*, *45*) as do multiple model compounds (*46*). A general trend in the stability of transition-metal complexes (Mn < Fe < Co < Ni < Cu > Zn; the Irving-Williams series) has received theoretical justification on the basis of ionic radii and second ionization potentials (*31*). The net effect of such factors may be visualized as leading to a relative shift between the two Bari centers shown in Figure 2A. We also note that hydrated Zn^{2+} and Co^{2+} ions in solution, assumed above to be of the form $M^{2+}(H_2O)_6$, may to different extents undergo octahedral-tetrahedral equilibria (*47*); to the extent that tetracoordinate Co^{2+} occurs, such differences would scale the LFSE term but not alter its essential character.

II. Experimental Characterization of WT1-p. A model finger of biological interest is provided by Wilms' tumor peptide WT1-p (finger 3; *12*). The present studies employ a 29-residue synthetic peptide (Figure 4A). The peptide contains putative ligands (C5, C8, H21, and H25; green in Figure 4A,B) and framework side chains (F3, F12, and L21; blue and red) in accord with the classical consensus sequence (*2*). The sequences of WT1 fingers 2−4 are homologous to fingers 1−3 of Zif268. The two proteins recognize related DNA sites and exhibit similar modes of protein−DNA recognition (Figure 1A; *48*).

a. NMR Studies of WT1-p. ^{1}H NMR spectra of the Zn^{2+}- and Co^{2+}-peptide complexes are shown in Figure 4B,C. The spectrum of the Zn finger (Figure 4B) exhibits conventional high-resolution features, whereas that of the Co finger (Figure 4C) exhibits the expected paramagnetic broadening and extreme shifts due to the bound high-spin cobalt ion (*49*). Sequential assignment of the Zn spectrum demonstrates that the peptide exhibits a canonical $\beta\beta\alpha$ fold in accord with multiple previous NMR studies of Zn fingers (*7*, *8*, *50*), including analysis of the intact WT1 DNA-binding domain by Wright and co-workers (*48*). Residues 1, 2, and 26−29 are not well ordered. As in other proline-containing fingers (*39*), major and minor conformations are observed consistent with slow exchange between *cis* and *trans* X−Pro peptide bonds (Supporting Information).

The WT1 domain (unlike previous classical fingers studied in this and other laboratories; *25*) contains no protected amide resonances after 5 min in D_2O solution at 25 °C (pD 6.2). At 4 °C fleeting protection of C8 H_N is detectable, consistent with formation of a canonical amide−sulfur hydrogen bond (*50*) (C5 $S_\delta \cdots H_N$ C8). Increasing the concentration of peptide and free Zn^{2+} does not prolong protection at this or other sites. NOESY spectra nevertheless exhibit a dense network of interresidue contacts.[5] Prominent contacts are observed among the side chains in the metal-binding site and hydrophobic minicore. These are in each case consistent with the crystal structure of the homologous finger in Zif268 (*3*). These include multiple contacts involving the Zn ligands and framework side chains F3, F12, and L18. The peptide contains a third histidine (H17) not involved in Zn^{2+} coordination; its chemical shifts and NOE contacts are readily distinguishable from those of H21 and H25. Although side chains on the surface of the finger generally exhibit fewer NOEs, the side chain of R14 (β, γ, and δ methylene protons) exhibits several contacts with the neighboring side chain of H17. Partial ordering of the DNA-binding surface (R14, D16, and H17) is in accord with NMR studies of an Sp1 Zn finger (*51*).

Although the absence of protected amide protons in D_2O provides evidence for breakage of hydrogen bonds on the time scale of seconds to minutes, the NOE network thus demonstrates maintenance of an ordered mean structure. Differences among amide proton exchange rates on the millisecond-to-second time scale are evident on comparison of amide resonance intensities following solvent presaturation and corroborated by observation of solvent exchange cross-peaks in NOESY spectra obtained in H_2O without solvent excitation (*40*; Supporting Information). Evidence for structural rigidity within the C-terminal α-helix and metal-binding site is provided by observation of an unusual exchangeable T22 δ-OH resonance at 5.4 ppm. This resonance exhibits TOCSY connectivity to T22 δ-CH_3 and NOESY contacts to this and neighboring methyl groups (L18). Although not protected in D_2O on a time scale of minutes, observation of a discrete −OH resonance in slow exchange with solvent water implies formation of a hydrogen bond stability maintained for at least 5 ms. The crystal structure of Zif268 and the present distance-geometry models (see below) indicate the presence of a bifurcated helix-related hydrogen bond between T22 δ-OH and the carbonyl oxygen of L18 and both the amide group and δ-OH function of T22 (Supporting Information).

Resolution of interresidue NOEs is facilitated by homonuclear 3D NMR spectroscopy as illustrated in Figure 5. The TOCSY−NOESY spectrum permits, for example, a key long-range NOE in the core (F3 $H_{\beta 3} \rightarrow$ F12 H_N) to be resolved at the F3 H_α TOCSY editing frequency (Figure 5D). The large number of NOEs tightly constrains the structure even in the absence of hydrogen-bond restraints as ordinarily inferred from D_2O protection experiments. A high-resolution structure of the isolated finger (Figure 5A) has thus been calculated on the basis of 466 restraints (20 restraints per residue in the ordered moiety, residues 3−25; Table 2). The ensemble exhibits pairwise root-mean-square (RMS) deviations of 0.41 Å (main chain) and 1.50 Å (side chain); deviations are given by residue in Figure 6B. The solution structure is essentially identical to the homologous domain in the Zif268−DNA complex (shown in red in Figure 6A; *3*); RMS deviations between the solution structure of the WT1 domain and crystal structure of the Zif268 domain are provided in the Supporting Information.[6] The geometry of the Zn-binding site (ligand−metal bond angles and ligand−ligand distances) are similar but not identical to that of Zif268 finger 2 (Supporting Information); structural parameters lie within the range observed among a collection of crystal

[5] ZFY-derived fingers (*39*) exhibit protected amide protons despite weaker affinity for Zn^{2+} (*25*). This discordance highlights the distinction between thermodynamic stability and conformational fluctuations.

[6] The sequence of the homologous Zif268 domain is (N) KPFQC*RI*C-*MRN*FSRSDHL*TTHI*RTHTG (finger 2); nonconserved residues are italic.

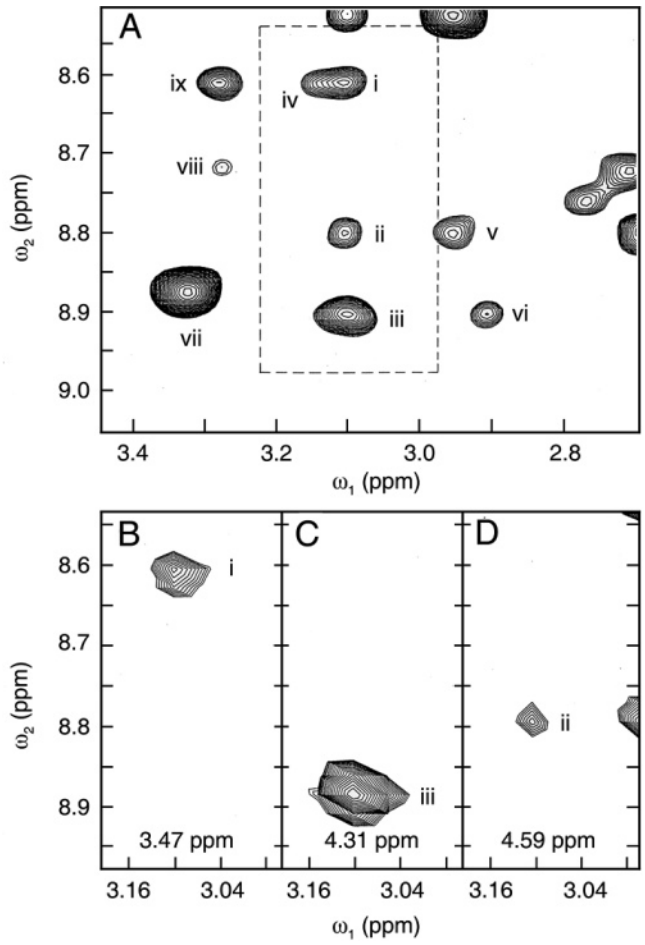

FIGURE 5: Sections of homonuclear 2D NOESY and 3D TOCSY−NOESY NMR spectra of the WT1-p Zn finger. (A) Region of the 2D NOESY spectrum exhibiting overlap in the ω_1 dimension. Overlapping resonances are labeled in Roman numbers (i−ix) as follows: S15 H_α to H_N (i), F3 $H_{\beta 3}$ to F12 H_N (ii), and H21 $H_{\beta 3}$ to T22 H_N (iii). Other cross-peaks in the region include S15 H_N to H_α (minor conformation) (iv), F3 $H_{\beta 2}$ to F12 H_N (v), H21 $H_{\beta 2}$ to T22 H_N (vi), T7 H_β to T7 H_N (vii), $SH_{\beta 3}$ to D16 H_N (viii), and S15 $H_{\beta 3}$ to S15 H_N (ix). Dotted lines indicate the region shown in panels of the 3D NMR spectrum in the corrresponding 2D cross planes: (B) The 2D plane at S15 $H_{\beta 2}$ frequency shows S15 H_α to S15 H_N connectivity (i), (C) the H21 H_α plane shows H21 $H_{\beta 2}$ to T22 H_N connectivity (ii), and (D) the F3 H_α plane shows F3 $H_{\beta 3}$ to F12 H_N connectivity (iii). In panel A the NOESY mixing time was 200 ms; in panels B−D the NOESY and TOCSY mixing times were 200 and 40 ms, respectively.

structures. The positions of L18 and T22 are consistent with formation of bifurcated L18 C═O···HO_γ T22 and L18 C═O···H_N T22 hydrogen bonds (not input into the restraints). In addition, the proximity and orientation of R14 and D15 on the surface of the fingertip (red box in Figure 6A) suggest the presence of a salt bridge, foreshadowing the network of hydrogen bonding in the classical Zn finger−DNA interface (*3*, *51*).

b. Raman Studies of Metal-Dependent Peptide Folding. Although it is not feasible to determine the solution structure of the Co finger due to paramagnetic perturbations (*49*), its similarity to the Zn finger is indicated by laser Raman spectroscopy. Unlike NMR resonances, Raman vibrational bands are not broadened or shifted by the magnetic properties of high-spin cobalt. The amide I region of the Raman spectrum exhibits essentially identical metal-dependent folding transitions on binding either Zn^{2+} or Co^{2+} (Figure 7A,B). The amide I bands of the Zn and Co fingers also exhibit similar line widths, a probe of main-chain dynamics (*30*). In accord with a previous Raman study of a Zn finger (*52*), the features near 1657 cm^{-1} in the difference spectra shown in the upper two traces in Figure 7B demonstrate a large change in secondary structure. In these traces the positive band near 1603 cm^{-1} is due to a Zn−His or Co−His mode (*52*), while the negative feature near 1575 cm^{-1} is due to free His in the apoprotein. Deconvolution of these spectra (Table 3) suggests a transition to a mixture of α-helix and β-sheet in accord with the ββα motif. The results of the deconvolution are very similar for the Zn^{2+} and Co^{2+} fingers. The double-difference spectrum (bottom trace in Figure 7B) is remarkable only for a feature at 1606 cm^{-1}, consistent with differential effects of the two metal ions on a ring mode of histidine. The similarity of Raman spectra is in accord with the crystal structure of a Co finger−DNA complex (in which canonical ββα structures were observed; *53*) and with the general correspondence between crystal structures of cobalt and zinc metalloenzymes (*1*, *54*).

c. Calorimetric Studies of Metal Ion Binding. ITC provides a direct test of an enthalpy-driven mechanism. The observed thermodynamics of metal ion binding reflect (i) its desolvation and protein coordination, (ii) coupled peptide folding, and (iii) associated changes in buffer ionization (*25*). In accord with X-ray structures (*53*) and the present Raman study, we assume that the peptide adopts a similar structure on binding either Zn^{2+} or Co^{2+}. The apparent enthalpy of observed heat, ΔH_{obs}, contains contributions from the intrinsic enthalpy of binding and the enthalpy of ionization of the buffer (*55*):

$$\Delta H_{obs} = \Delta H_{binding} + N_{H^+}\Delta H_{ioniz} \quad (5)$$

where N_{H^+} designates the number of protons released (if $N_{H^+} > 0$) or bound (if $N_{H^+} < 0$) by the buffer upon metal-dependent peptide folding. Because the present ITC studies employ the same buffer in titration of either metal ion, the ΔH_{ioniz} terms are constant. We also assume that N_{H^+} is also the same, as in each case a solvated metal ion becomes bound to the same peptide ligands. Observed thermodynamic differences then simplify to reflect buffer-independent quantities:

$$\Delta\Delta H_{obs} = \Delta\Delta H_{binding} + \Delta N_{H^+}\Delta H_{ioniz} = \Delta\Delta H_{binding} \quad (6)$$

Representative ITC data are shown in Figure 7C,D. Comparison of Zn^{2+} and Co^{2+} ITC titrations yields an affinity difference ($\Delta\Delta G$) of 3 kcal/mol (Table 4). Within experimental error the origin of this difference is purely enthalpic.[7]

DISCUSSION

Understanding the physical origins of the thermodynamic properties of proteins poses a major problem in structural biology. Despite an exponential increase in structural information, the ability to predict stabilities and ligand affinities

[7] The strength of Zn^{2+} binding is within the calibration range of the instrument but near its tight-binding limit. Any possible underestimate in its association constant would accentuate the degree of noncompensation: metal-binding selectivity could be augmented rather than mitigated by possible entropic differences.

Table 2: Statistical Parameters for WT1-p

interresidue NOEs	440	dihedral angle restraints	24
sequential	155	ϕ	12
medium-range	135	χ_1	12
long-range	150	hydrogen bonds[a]	2
mean restraint violations		deviations from ideal covalent geometry	
NOE violations (Å)	0.01	bond length deviations (Å)	0.008
dihedral violations (deg.)	0.19	bond angle deviations (deg)	2.67
main-chain RMSD[b] (Å)	0.41	side-chain RMSD[b] (Å)	1.50
empirical energies (kcal/mol)		empirical energies (kcal/mol)	
NOE restraint energy	0.1 ± 0.2	constrained dihedral	2.2 ± 0.5
van der Waals	3.3 ± 0.9	covalent bond lengths	5.1 ± 0.4
improper dihedral	12 ± 3	bond angles	89 ± 2.0

[a] A single hydrogen bond was imposed on the basis of observation of a protected C8 amide resonance in D_2O solution and preliminary DG/SA calculations; two distance restraints were imposed as described (*50*). [b] RMS deviations were calculated for residues 3−25 only on the basis of an alignment of the main-chain atoms of these residues.

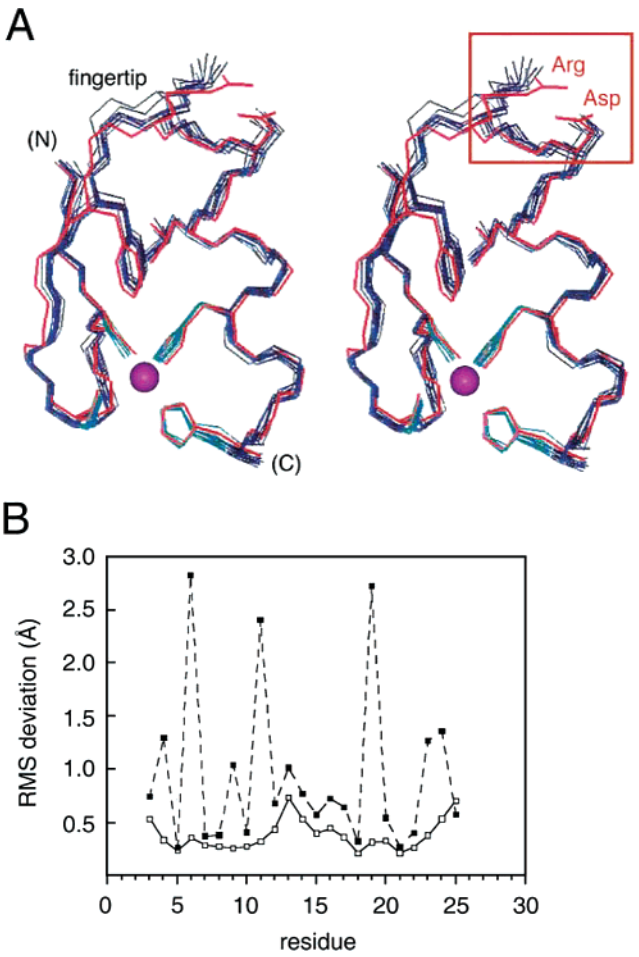

FIGURE 6: Solution structure of WT1-p. (A) Solution structure of WT1 Zn finger 3 based on homonuclear 2D and 3D NMR spectroscopy (stereopair). The structure is similar to the crystal structure of the homologous finger in a specific Zif268−DNA complex (shown in red; Protein Data Bank entry 1ZAA; *3*). The Arg-Asp DNA recognition element is boxed. Chemical shifts and restraints used in distance geometry/simulated annealing calculations are provided in the Supporting Information. (B) Root-mean-square deviations of the ensemble. RMSDs are shown by residue between all pairs of structures in the WT1 ensemble for the backbone (open squares) and side chain (filled squares) heavy atoms. RMS deviations were calculated by pairwise comparison and not in reference to a common mean structure (which would yield smaller numbers).

has remained limited. Although this limitation in part reflects the size and complexity of proteins, even in apparently simple cases chemical intuition can be misleading. The enhanced Ca^{2+} affinity of multivalent organic acids, for example, is not a consequence of the long-postulated entropic "chelate effect" (*56*) but instead is enthalpic in origin (*18*, *57*). The thermodynamics of binding metal ions to globular proteins likewise exhibits hidden complexity (*16*, *17*), making enthalpic and entropic driving forces difficult to distinguish. Such distinctions are further confounded by EEC, observed in a wide range of chemical and biochemical processes (*19*−*24*). In this study we have investigated the hidden thermodynamics of the zinc finger, a peptide cage containing a tetrahedral Zn^{2+}-binding site (*2*, *7*, *8*, *58*, *59*). Why are perturbations in the framework of a Zn finger offset by EEC to restore its stability (*25*) whereas changes in the identity of the metal ion are not? Given the general preference of Zn fingers and other zinc metalloproteins for Zn^{2+} relative to Co^{2+}, why does the extent of metal ion selectivity (the ratio of Zn^{2+} to Co^{2+} association constants) exhibit significant variation?

Although seemingly contained within the realm of inorganic chemistry (*9*, *11*), the properties of metalloproteins are deeply connected to the evolution of the biosphere (*10*, *60*). The advent of aerobic organisms was associated with a profound change in the chemistry of the earth, including in the abundances of transition-metal ions and their complexes (*61*). Although zinc is today the most common trace metal ion in the cytoplasm of eukaryotic cells, it was likely to have been rare ($<10^{-13}$ M) in primordial anaerobic seas and ponds of the Archean era (3.4−2.8 billion years ago) as the presence of sulfides would have led to its precipitation (*10*, *62*). Cobalt ions would have been more abundant (10^{-12} M), and unlike zinc, their soluble sulfide clusters could have been of biological utility. Cobalt-dependent enzymes are now rare but essential relics of this anaerobic world (*10*, *63*). The oxygen-dependent transition from sulfide to sulfate chemistry in seas of the Proterozoic era (2500−543 million years ago; *64*) permitted the concentration of zinc ions to rise more than 10^5-fold (*10*). Whereas in an era of zinc scarcity metal-binding affinities must have been high (association constant $K_a > 10^{10}$ M^{-1}) and associated with well-organized apoprotein structures, the increased availability of zinc ions would have provided an opportunity for the evolution of lower affinity Zn modules: globular minidomains whose folding is coupled to zinc coordination ($K_a = 10^7 - 10^9$ M^{-1}). To extend the study of a consensus Zn finger of optimal design and high affinity (CP-1; *14*), we have therefore chosen to investigate a natural finger of lower thermodynamic stabil-

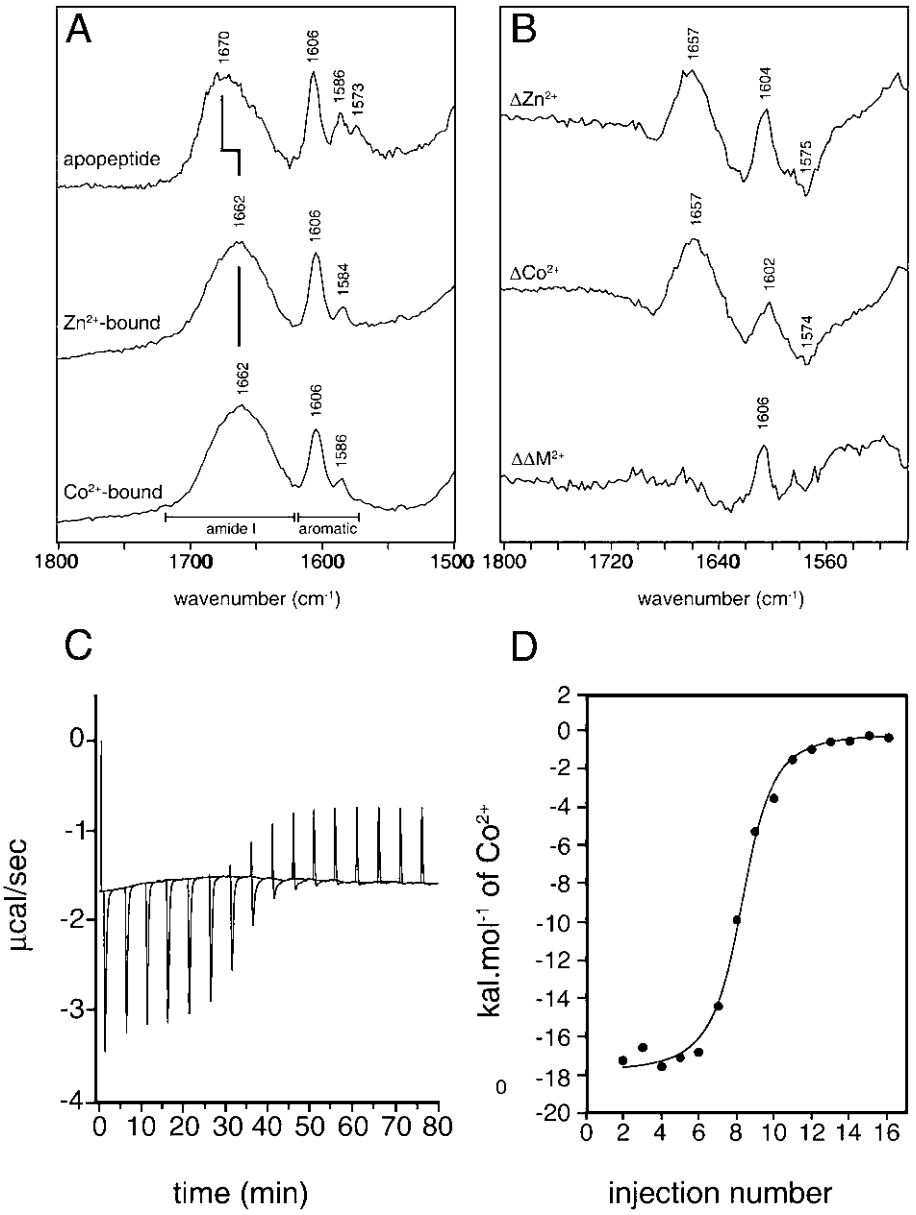

FIGURE 7: Raman analysis and representative ITC titration. (A, B) Raman studies of WT1-p apopeptide and metallo complexes. (A) Amide I and aromatic bands. Spectra of the Zn^{2+}-bound and Co^{2+}-bound fingers (middle and bottom panels) are similar but differ markedly from the spectrum of the apopeptide (top). The peak of the amide I band shifts from 1670 cm^{-1} in the apopeptide to 1662 cm^{-1} in metallopeptide complexes (vertical line). The band at 1606 cm^{-1} arises from the side chain of Phe and His; bands at 1573−1586 cm^{-1} are from His. (B) Raman difference spectra. Metal-dependent folding transitions are similar for Zn^{2+} and Co^{2+} complexes (top and middle traces). Difference features reflect the transition of disordered coil to α-helix (peak at 1657 cm^{-1}) and metal binding to imidazole rings of histidine (1574−1604 cm^{-1}). The difference spectrum between Zn^{2+}-bound and Co^{2+}-bound fingers (bottom) is negligible in the amide I region and exhibits an aromatic difference feature at 1606 cm^{-1} assigned to a ring mode of histidine bound to the metal ion. (C, D) ITC studies of the consensus apopeptide with $CoCl_2$ in 50 mM HEPES buffer (pH 6.5) at 25 °C. The peptide concentration was 10 μM. The solid line in (D) represents a fit to the data by a one-site model.

ity: WT1-p derived from the human tumor-suppressor protein WT1 (*13*, *28*). Although the mean structure of WT1-p is essentially identical to crystal structures of homologous domains (*3*) and hence closely resembles CP-1, WT1-p (unlike CP-1) lacks protected amide protons in D_2O solution and so exhibits significant subglobal conformational fluctuations.

Strengths and Limitations of the Ligand-Field Viewpoint. The strengths of the LFSE model are its simplicity and universality (*9*). Because the proposed mechanism invokes only general geometric features of the metal-binding site and the electronic structure of transition-metal cations, the LFSE penalty incurred on binding of Co^{2+} (but not Zn^{2+}) is robust to other details of protein structure and dynamics. The resulting difference in peptide-metal ion association constants is purely enthalpic as demonstrated by an elementary statistical-thermodynamic model (section I of the Results). These elegant strengths do not, however, ensure the *predominance* of LFSE relative to other possible thermodynamic contributions to metal ion selectivity, nor can LFSE itself account for variation in selectivity ratios (Table 1). Metal-dependent changes in protein structure, for example, may be accompanied by complex changes in the entropic and enthalpic origins of protein stability, which in general will

Table 3: Raman Analysis of WT1-p: Gaussian Deconvolution of Amide I Bands[a]

sample	1654 cm^{-1}	1681 cm^{-1}	1664 cm^{-1}
Zn^{2+}-peptide	36 ± 3	33 ± 4	31 ± 7
Co^{2+}-peptide	30 ± 3	39 ± 1	31 ± 3

[a] Values are given as percentages. Fitting employs three Gaussian bands centered at 1654, 1681, and 1664 cm^{-1}. The former is ascribed to peptides in α-helical space; the latter two are due to β-sheet contributions and residues in Ramachandran β space but not in extended sheets (*88*). An alternative interpretation is that the 1664 cm^{-1} band is due to random coil and the 1681 cm^{-1} band is due to β sheet and turn contributions (*89*, *90*). We also fitted the amide I profile using the method of Berjot (*91*) that uses a basis set of 15 globular proteins; this gave 36 ± 1% for α-helix, 43 ± 1% for β-sheet, and 20 ± 1% for random and turn contributions from both Zn^{2+} and Co^{2+} bound peptides.

be accompanied by thermodynamic compensation. Indeed, Berg and co-workers (*14*) have ascribed the anomalous thermodynamic properties of CAII (Figure 3A; *17*) to putative conformational changes on metal ion exchange not evident on comparison of high-resolution crystal structures (*65*−*67*). Toone and colleagues have by contrast attributed the greater change in enthalpy observed on binding of Co^{2+} to CAII (relative to Zn^{2+}) to the difference between their respective enthalpies of hydration. We will consider these divergent perspectives in turn.

Metal Ion Selectivity and Energy Landscapes. The LFSE model is an approximation as even in the absence of conformational changes in the metalloprotein it neglects intrinsic differences between metal ions. Such differences may be marked (as between Zn^{2+} and Cd^{2+}, each without LFSE penalties) or subtle (as between Zn^{2+} and Co^{2+}, essentially isosteric replacements). Indeed, the trend of the Irving−Williams series of stabilities of transition-metal complexes (Mn < Fe < Co < Ni < Cu > Zn) highlights the decrease from Cu^{2+} to Zn^{2+}, which leads to similar but not identical stabilities among octahedral Zn^{2+} and Co^{2+} complexes. We may express the difference between stabilities of Zn and Co fingers as the sum of LFSE ($\Delta\Delta G_{LFSE}$), Irving−Williams terms ($\Delta\Delta G_{I-W}$), and possible structural reorganization in the protein ($\Delta\Delta G_p$):

$$\Delta\Delta G = \Delta\Delta G_{LFSE} + \Delta\Delta G_{I-W} + \Delta\Delta G_p \approx \Delta\Delta H_{LFSE} + \Delta\Delta G_{I-W} \quad (7)$$

We assume that the peptide structures of Zn and Co fingers are essentially identical and hence exhibit similar intramolecular energies (exclusive of metal ion interactions) in their ground states:

$$\Delta\Delta G \approx \Delta\Delta H_{LFSE} + \Delta\Delta G_{I-W} = \epsilon + \Delta\Delta G_{I-W} \quad (8)$$

Further, because diverse Zn fingers exhibit similar tetrahedral metal-binding sites and hence LFSE penalties (ϵ) on binding Co^{2+}, the observed variation among ratios of Zn^{2+} to Co^{2+} association constants (including that between CP-1 and WT1-p; Table 4) must arise from differences between corresponding $\Delta\Delta G_{I-W}$ terms, and these differences (like those due to LFSE) seem not to incur significant EEC.

Irving−Williams terms (such as the respective electron affinities of Zn^{2+} and Co^{2+} ions) surely contribute to the relative stabilities of peptide−transition-metal complexes, but why would such contributions differ from finger to finger? We suggest that such differences arise from the topographies of the underlying energy landscapes of peptide folding (*32*, *33*). Whereas CP-1 exhibits exceptional thermodynamic stability within a rigid peptide framework, WT1-p is significantly less stable, and its elements of secondary structure exhibit rapid conformational fluctuations, leading to amide proton exchange. The landscape of CP-1 is thus deep and narrow, whereas that of WT1-p (at least near its bottom) is shallow and broad (Figure 8). We now compare corresponding landscapes between Zn and Co fingers (black and red surfaces in Figure 8). Interchange of metal ions leads to an upward displacement of the landscape ($\Delta\Delta E_1$ and $\Delta\Delta E_2$ in Figure 8) due to both LFSE (ϵ) and Irving−Williams terms ($\Delta\Delta H_1$ and $\Delta\Delta H_2$). Because folding of a peptide cage imposes an allowed range of bond angles and bond lengths in the metal-binding site and because the stringency of this range varies with the landscape, respective Irving−Williams terms may not be identical ($\Delta\Delta H_1 > \Delta\Delta H_2$). This argument rests on the assumption that subtle differences exist between the ideal ground-state tetrahedral coordination geometries by Zn^{2+} and high-spin Co^{2+} that are tolerated or overridden to different extents (Δr_1 and Δr_2 in Figure 8) by the matrix of surrounding peptide interactions. EEC would be negligible only in the limit of small and localized structural adjustments without an overall change in the landscape topography. Nonnegligible EEC (as observed in studies of CAII; *17*) may occur following significant structural reorganization (as proposed by Blasie and Berg (*14*)) or due to nonlocal coupling between the metal-binding site and the environment as considered below.

Open and Closed Metal-Binding Sites. The Zn finger is remarkable for the economy of its structure. Encagement of Zn^{2+} or Co^{2+} by two histidine and two cysteate side chains creates a sealed environment. By contrast, metalloenzymes often contain a catalytic metal ion that is partially exposed to solvent (or substrate) and hence available to participate in the reaction mechanism (*1*). The Zn^{2+} ion at the bottom of the active-site cleft of CAII, for example, is incompletely coordinated by three histidine side chains (*65*, *67*) (Figure 3A). The fourth ligand is a solvent-derived hydroxide ion (or water molecule), which is in turn hydrogen-bonded to the γ-hydroxyl group of a threonine. Whereas CAII binds Zn^{2+} 24000-fold more tightly than Co^{2+}, ITC analysis has demonstrated that factors other than LFSE must predominate in determining these relative affinities (*17*): metal ion selectivity ($\Delta\Delta G$ = 5.9 ± 0.9 kcal/mol) is driven by differences in *entropy* ($T\Delta\Delta S$ = 15.3 ± 2.1 kcal/mol) with incomplete enthalpic compensation ($\Delta\Delta H$ = 9.4 ± 0.3 kcal/mol). Despite structural similarities between the Zn^{2+}- and Co^{2+}-bound enzymes (*54*, *68*), the change in entropy on binding of Zn^{2+} is positive ($T\Delta S$ = 7.8 ± 0.4 kcal/mol) whereas that incurred on binding of Co^{2+} is negative and nearly equal in magnitude ($T\Delta S$ = −7.5 ± 1.7 kcal/mol). This marked difference presumably reflects complex coupling between the metal-binding site and a reservoir of interactions within the protein core (mediated by "second-shell" side chains) and in turn with changes in solvent reorganization (*17*). Although comparable thermodynamic analyses of other metalloenzymes are not available, an additional example of a metal ion in an "incomplete" environment is provided by the Zn−insulin hexamer: three

Table 4: ITC Analysis of WT1-p

metal ion	K_a (M^{-1})	ΔG (kcal/mol)	ΔH (kcal/mol)	$T\Delta S$	$\Delta\Delta G$	$\Delta\Delta H$
			A. WT1[a]			
Zn^{2+}−WT1	$(5.5 \pm 1.0) \times 10^8$	−11.9	−21.2 ± 0.4	9.3 ± 0.4		
Co^{2+}−WT1	$(3.7 \pm 0.6) \times 10^6$	−9.0	−17.9 ± 0.3	8.9 ± 0.3	−2.9	−3.3 ± 0.7
			B. CP-1[b]			
Zn^{2+}−CP-1		−16.0	−23.4 ± 1.0	7.4 ± 1.0		
Co^{2+}− CP-1		−9.8	−15.9 ± 2.0	6.3 ± 2.0	−6.2	−7.5 ± 3.0

[a] Values were obtained in 50 mM HEPES−HCl buffer (pH 6.5 and 25 °C). Data are derived from the mean of two individual experiments as described (*25*). The errors shown are those associated with the nonlinear least-squares fitting of the enthalpy. The observed Zn^{2+}:peptide and Co^{2+}:peptide stoichiometries were unity, and the determined heats of dilution, when subtracted, gave a baseline reading of zero enthalpy. Inferred values of $T\Delta S$ for binding of Co^{2+} and Zn^{2+} are −9.0 and −9.3 kcal/mol, respectively; these values are not distinguishable within experimental error. To ensure that Cys residues remained reduced, the peptide was dialyzed in a buffer that had been saturated with argon gas to displace dissolved O_2. Titrations were performed immediately after dialysis under airtight conditions. The small opening between the syringe and the cell mountings was sealed with Parafilm; a flow of N_2 gas was applied across the cell mounting throughout the experiment. [b] Values of ΔG were obtained from spectrophotometric titrations (*92*). Values of ΔH were obtained by ITC (*14*); values of $T\Delta S$ were inferred. $\Delta\Delta H$ values at pH values of 7.0, 6.0, and 5.5 are −7.5 ± 3.0, −7.7 ± 1.6, and 7.6 ± 1.6, respectively. ITC values were obtained in 50 mM Hepes-HCl buffer at pH 6.5 and 50 mM NaCl at 25 °C. The data above were uncorrected for proton release, assumed to be the same for Co and Zn fingers.

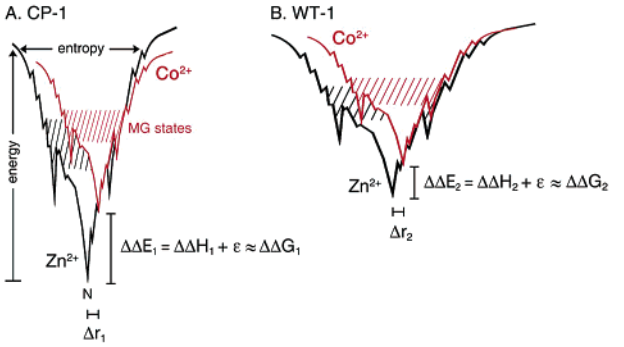

FIGURE 8: Proposed coupling between the thermodynamics of metal ion binding and topography of the energy landscape. Landscapes of Zn fingers are shown in black; corresponding landscapes of Co fingers are shown in red. Whereas consensus finger CP-1 folds within a deep and narrow funnel (A), WT-1-p exhibits a broader and less deep landscape (B) as indicated by its lower stability and enhanced rates of subglobal amide proton exchange. Hatched lines indicate molten-globule (MG) states. Differences in stability between Zn and Co fingers ($\Delta\Delta E_{1,2}$) depend on both the classical LFSE term ϵ (see section I of the Results) and coupling between Irving−Williams factors and the variable topography of the energy landscape ($\Delta\Delta H_{1,2}$; see the Discussion). The ratio of Zn^{2+} to Co^{2+} affinities thus varies among fingers (Table 1). Schematic depictions of energy landscapes are adapted from refs *32* and *33*: energy is represented by the vertical depth and entropy by the width of the funnel.

histidine side chains contact a structural metal ion (*69*) whose coordination is extended by solvent or other nonprotein-derived ligands (*70*). Binding of Zn^{2+} is entropy-driven (*71*), presumably due to coupled effects of protein assembly and solvent reorganization.[8]

Nominal and Environmental Perspectives. The contrast between the thermodynamics of CAII and a classical Zn finger highlight two divergent perspectives regarding the origin of EEC. One focuses on the structure and dynamics of the nominal system (*21*, *72*−*74*) and the other on the coupling between this system and its environment (*20*, *23*, *24*). The first perspective envisages a tradeoff between the strength of interactions at a noncovalent interface (such as a protein−ligand complex or within a hydrophobic core) and the entropic cost of its immobilization. This mechanism, essentially a gas-phase view, is intuitive and readily rationalized by consideration of tight and loose potential wells (*21*, *22*; Figure 2A). The extent of EEC would reflect the depth of the potential well and density of states within the well (relative to k_BT). The second perspective is motivated by solvation phenomena (*22*−*24*, *75*) as compensation arises naturally in theoretical models of solvent−solvent and solvent−solute interactions (*24*, *76*, *77*). Changes in solvent reorganization lead to compensating terms in general expressions for partial molar entropy and enthalpy, and these contributions are proposed to dominate changes within the apparent object of study (*24*) (which may be noncompensating).

Recent theoretical studies have illuminated the general principle that coupling of a nominal system to a fluctuating environment leads, on small perturbations, to compensating terms in expressions for the partial molar entropy and enthalpy (*19*, *78*, *79*). Perturbations in hydrophobic solvation provide a physical realization of this formalism, but its application does not depend on the special properties of water. Compensation is likely to occur generally in systems with large fluctuations and high densities of states. An instructive toy model of EEC has been described by Qian (*80*) based on an ideal gas with a fluctuating boundary constrained by a spring (Figure 9A). Intended as a toy protein, this model exhibits EEC due to an "induced fit": fluctuations in volume and pressure of the gas due to its environmental coupling. Compensating terms in expressions for partial molar entropy and enthalpy are proportional to the thermal expansivity α:

$$\alpha = \frac{p^2}{T(p^2 + \eta N k_B T)} \qquad (9)$$

where N indicates the number of gas particles, p the pressure, η the spring constant, T the temperature, and k_B Boltzmann's

[8] The Zn−insulin hexamer contains two axial Zn^{2+} ions, one per trimer. The coordination geometry of the bound metal ions in insulin hexamers can reversibly switch from tetrahedral to octahedral on addition of salt or phenolic ligands (*98*) (the T → R transition). High-resolution crystal structures have in some cases demonstrated partial occupancy of both tetrahedral and octahedral geometries at the same site (*70*). Although thermodynamic differences ($\Delta\Delta H$ and $T\Delta\Delta S$) between Zn^{2+}- and Co^{2+}-coordinated hexamers have not been investigated, a pure LFSE-driven mechanism of metal ion selectivity would not be anticipated due to complex conformational effects.

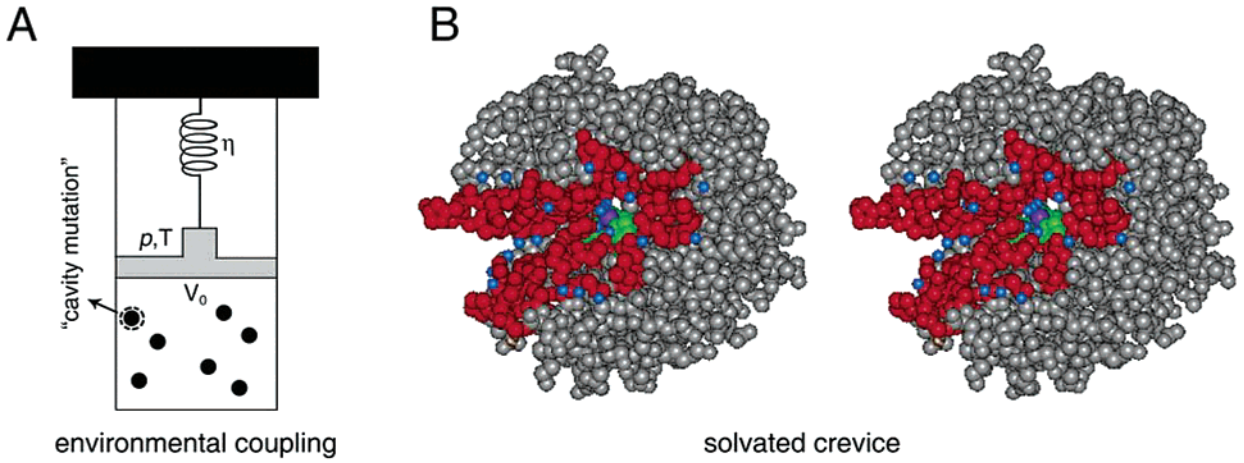

FIGURE 9: (A) Elementary model of an ideal gas in a piston whose volume is influenced by the external pressure p and a fluctuating boundary due to a spring with Hooke constant η. The equilibrium position of the piston is given by $V_o = Nk_BT/p$. Removal of a molecule from the gas (dashed circle) would be associated with changes in volume, enthalpy, and entropy. Compensating terms in expressions for changes in molar entropy and enthalpy are related to the work $p\Delta V$. The volume change in the fluctuating boundary ensemble is proposed to be analogous (*80*) to a conformational change in a protein and its solvation in response to a cavity-forming mutation (*93*) and is the origin of compensating terms in the partial molar entropy and enthalpy of the system. This panel is adapted from Qian (*80*). (B) Hydration of the active-site cleft in CAII. Atoms lining the cleft are shown in red, bound water molecules are shown in blue, the catalytic zinc ion is shown in purple, and inner-shell protein ligands are shown in green. The structural basis of EEC in CAII is not understood in detail.

constant. This term vanishes in the limit of a completely rigid "spring" ($\eta \rightarrow \infty$), in which case volume fluctuations are absent (*80*). An analogy is proposed between removal of a gas molecule (arrow in Figure 9A) and a mutation in a protein. In this model the presence of EEC in a ligand-exchange reaction would depend on the extent of coupling between the site and the spring.

Relationship between LFSE and Enthalpies of Hydration. Respective enthalpies of binding of metal ions to CAII differ ($\Delta H_{Co(II)} = -18 \pm 1$ kcal/mol; $\Delta H_{Zn(II)} = -8.6 \pm 0.2$ kcal/mol). That binding of Co^{2+} is significantly more exothermic (*17*) ($\Delta\Delta H = -11.6$ kcal/mol) is inconsistent with the LFSE model. This discrepancy was hypothesized by Toone and colleagues to arise in part from differences in the intrinsic enthalpies of hydration of the metal ions (*81*) ($\Delta\Delta H_{hyd} = 4$ kcal/mol) as it is more difficult to remove inner-shell water molecules from $[Zn(OH_2)_6]^{2+}$ than from $[Co(OH_2)_6]^{2+}$ in accord with their relative nuclear charges. Although extracted from experimental data,[7] standard enthalpies of hydration refer to a *gedanken* experiment: the formal process of removing a hydrated metal ion from solution to obtain the naked ion in the gas phase.[9] According to standard values (*81*), hydration of Zn^{2+} is slightly more exothermic ($\Delta H_{hyd} = -507$ kcal/mol) than that of Co^{2+} ($\Delta H_{hyd} = -503$ kcal/mol). In studies of the molecular basis of metal ion selectivity by proteins, is such use of formal enthalpies of hydration appropriate, and if so, what is the relationship between this factor and LFSE? In the absence of other factors, consideration of enthalpies of hydration would predict—as a seeming paradox—that the Zn finger should bind Co^{2+} $\sim 10^3$-fold more tightly than Zn^{2+}. Alternatively, should enthalpic effects of LFSE and hydration be independent and additive, then the LFSE contribution (*59*) (−4.5 kcal/mol favoring Zn^{2+}) and the hydration term (*17*) (4.0 kcal/mol favoring Co^{2+}) would seem to cancel, leading to loss of metal ion selectivity. Neither of these predictions is in accord with experiment.

To discern why this reasoning is incomplete and to clarify the relationship between LFSE and enthalpies of hydration, we consider the following thermodynamic cycles. We first resolve the ligand exchange reaction (1 above) into its two component metal-dependent folding subprocesses:[10]

$$s_U{\cdot}P_U + s_M{\cdot}Zn^{2+} \leftrightarrows s_N{\cdot}P_N{\cdot}Zn^{2+} + s_b + \Delta N_{H^+} \quad (10a)$$

$$s_N'{\cdot}P_N'{\cdot}Co^{2+} + s_b' + \Delta N_{H^+} \leftrightarrows s_U{\cdot}P_U + s_M'{\cdot}Co^{2+} \quad (10b)$$

where s_b and s_b' refer to water molecules released or incorporated from bulk solvent, $s_{U,U}'$ and $s_{N,N}'$ to water molecules bound to the unfolded or native peptides, and s_M and s_M' to water molecules coordinating the metal ion, and ΔN_{H^+} refers to the number of protons released or bound (i.e., coupled to changes in buffer ionization). We will assume that these changes are identical in the two subprocesses and hence do not contribute to the ligand-exchange reaction. Because enthalpies of hydration refer to transfer of a metal ion from aqueous solution to the gas phase, we next imagine these processes as occurring in part in aqueous solution and in part in the gas phase (Figure 10). Although the coupled Co^{2+} and Zn^{2+} subcycles (respective left- and right-hand panels of Figure 10) appear more complex than the original ligand-exchange reaction and although use of gas-phase intermediates appears artificial, the complete cycle must yield equivalent values of $\Delta\Delta G$, $\Delta\Delta H$, and $T\Delta\Delta S$ since thermodynamic state functions are independent of the reaction pathway. For each metal ion the association or dissociation

[9] Although standard enthalpies of hydration are given in reference to formation of the formal H^+ ion in water (*97*) (see footnote 3), properties of the hydrogen ion cancel in consideration of difference values.

[10] For clarity we have omitted changes in ionization of the peptide on metal binding. In the gas phase this would formally be indicated by binding or release of H^+ ions, in solution by coupling to buffer ionization. Omission of these processes is justified by the assumption that they are identical on binding of Zn^{2+} and Co^{2+}, and so do not contribute to thermodynamic differences.

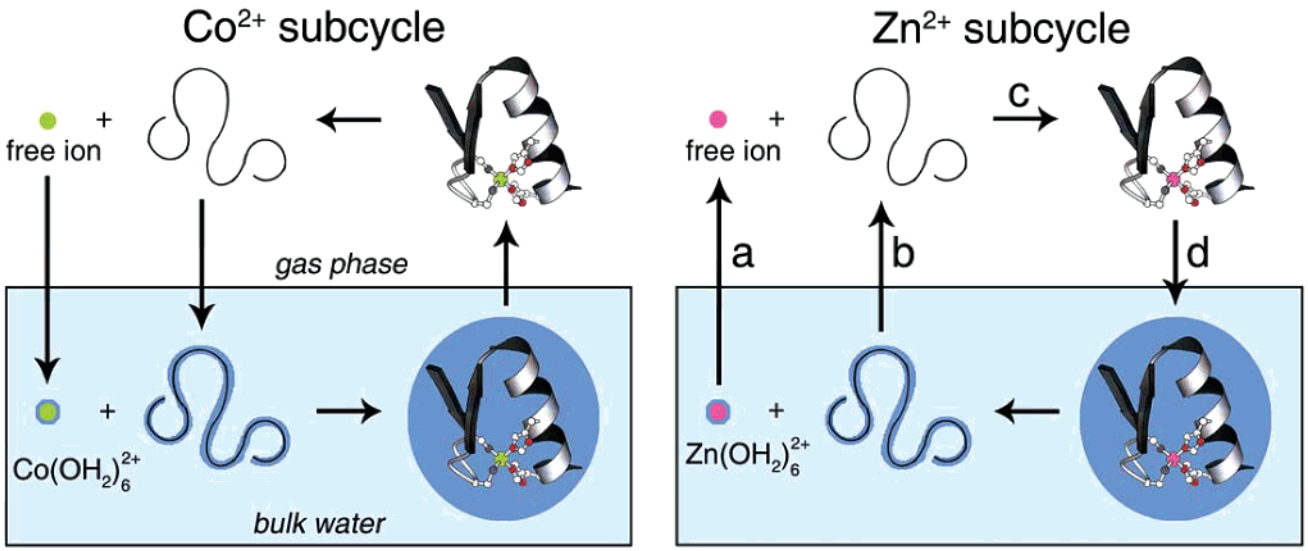

$$s_{N'} \cdot P_N \cdot Co^{2+} + s_M \cdot Zn^{2+} \leftrightarrows s_{M'} \cdot Co^{2+} + s_N \cdot P_N \cdot Zn^{2+}$$

FIGURE 10: Role of enthalpies of metal ion hydration in hypothetical thermodynamic cycles. The ligand-exchange reaction (bottom panel) can be decomposed into a Co^{2+} subcycle (left) and a Zn^{2+} subcycle (right). In each panel, the water bath is shown in light blue (rectangle) with gas-phase reactions depicted above. Co^{2+} is shown in green and Zn^{2+} in pink. Solvated apopeptides and metal−peptide complexes are surrounded by dark blue fields. Association/dissociation and solvation/desolvation subreactions (right-hand panel) are as described in the text (eqs 11a−d).

reaction may itself be viewed as the sum of four parts as follows:

$$M(OH_2)_6^{2+} \leftrightarrows (M^{2+})_{gas} + 6H_2O \quad (11a)$$

$$s_U \cdot P_U \leftrightarrows (P_U)_{gas} + s_U \cdot H_2O \quad (11b)$$

$$(M^{2+})_{gas} + (P_U)_{gas} \leftrightarrows (M^{2+}-P_N)_{gas} \quad (11c)$$

$$(M^{2+}-P_N)_{gas} + s_N \cdot H_2O \leftrightarrows (M^{2+}-P_N)_{solution} \quad (11d)$$

where M^{2+} indicates the metal ion. Four analogous subreactions underlie the association or dissociation of the second metal ion (designated subreactions 11a′-d′). Subreactions a and a′ contain the enthalpies of dehydration of the metal ions; differences between standard values indeed predict that dehydration of Zn^{2+} would be more endothermic than dehydration of Co^{2+} as indicated by Toone and colleagues (*17*). Whether this term can account for the puzzling thermodynamics of CAII, however, requires consideration of the entire cycle. We may omit analysis of subreactions b, b′, d, and d′ (solvation of the free and metal-bound peptides) as their net contribution to ΔΔ values is expected to be negligible.[11]

We first consider the meaning of standard enthalpies of hydration. Many factors may in principle contribute to subreactions a and a′, including the respective ionic radii, degree of shielding of the nuclear charge, and electrostriction in the surroundings of the solvated ion. Given the difference in nuclear charge between Zn^{2+} and Co^{2+}, why are their standard enthalpies of hydration so similar? *The expected difference in* ΔH_{hyd} *is almost completely offset by implicit LFSE terms*.[12] This can be seen by shifting our point of reference from the Bari center (upper dashed line in Figure 2A) to the energy level of the degenerate d orbitals of the gas-phase metal ion (lower dashed line in Figure 2A). Hydration of Zn^{2+} elevates all 10 d electrons and so fills both the lower (t_{2g}) and upper (e_g) sets of split orbitals in an octahedral field, yielding the mean Bari energy. Hydration of Co^{2+} leaves the upper levels half-filled, implying that the mean orbital energy is lower than the Bari center. Thus, LFSE terms implicitly enter into the standard enthalpies of hydration for *both* Zn^{2+} and Co^{2+}, but the incomplete d shell of Co^{2+} "rescues" the relative stability of the hydrated metal ion (relative to the gas phase). Similar reasoning applies to subreactions c and c′, which describe binding of the respective desolvated metal ion within the coordination environment of the polypeptide (gas-phase chelation). Like initial dehydration, the thermodynamics of peptide chelation is metal-dependent and implicitly contains LFSE terms, in this case a transition from degenerate d orbitals of the gas-phase ion to a tetrahedral ligand field. For Zn^{2+} this term exactly cancels that contained in the enthalpy of hydration, so no net LFSE penalty accompanies its transition from solvent to finger. For Co^{2+} cancellation does not occur, as a net LFSE penalty arises from the difference between LFSE terms intrinsic to the subprocesses of dehydration and chelation (a′ and d′, respectively).

[11] The second and fourth parts of the Zn^{2+} and Co^2 subcycles (subreactions 11b,d and 11b′,d′, respectively) would each be associated with an enthalpy and entropy of desolvation. Terms involving the apopeptide would exactly cancel in the overall ligand-exchange reaction. Terms involving the folded fingers would also cancel if the Zn^{2+} and Co^2 complexes should exhibit identical structures, dynamics, and patterns of solvation (as assumed in the LFSE model).

[12] The ΔH_{hyd} of Mn^{2+} (−458 kcal/mol) is 10% less than that of Zn^{2+} (−507 kcal/mol; *81*). Mn^{2+} exhibits a d^5 configuration with a weak ligand field and hence negligible LFSE. Linear extrapolation from Mn^{2+} to Co^{2+} predicts an LFSE-independent estimate of ΔH_{hyd} of −487 kcal/mol. The higher standard value for Co^{2+} (−503 kcal/mol) thus implies an implicit LFSE contribution of approximately −16 kcal/mol. Given the approximate nature of this calculation, this is in good agreement with the observed LFSE of the $[Co(OH_2)_6]^{2+}$ ion of −21.3 kcal/mol (*59*).

Hidden Thermodynamics of Metal-Ion Selectivity. The present study in part supports the insightful proposal by Berg and co-workers that the metal ion selectivity of the Zn finger reflects effects of LFSE (*9*) but also highlights the role of classical Irving−Williams terms (*31*). Our considerations further suggest that it is inappropriate to focus on enthalpies of hydration as direct indicators of enthalpic changes in the binding of transition-metal ions to proteins. Although it is indeed more difficult to dehydrate $[Zn(OH_2)_6]^{2+}$ than $[Co(OH_2)_6]^{2+}$, this difference is largely offset on binding of the metal ions to the peptide. Rather than being alternative viewpoints, the hydration−enthalpy model implicitly contains LFSE and Irving−Williams terms but yields an incomplete description of the thermodynamic cycle. The approximate success of the LFSE estimate in the case of a Zn finger (*9*) arises from the structural similarity between Zn^{2+}- and Co^{2+}-bound fingers, which leads to similar non-LFSE-related terms in the coupled cycles illustrated in Figure 10. Although the same LFSE terms must of physical necessity arise in the binding of Zn^{2+} and Co^{2+} to CAII, the anomalous thermodynamic features of this metalloenzyme demonstrate that differences in non-LFSE-related terms are nonnegligible, i.e., Co^{2+}- and Zn^{2+}-coordinated CAII complexes differ in other ways, and that these features dominate their thermodynamic differences. Such differences are also implied by inequivalent changes in heat capacity (ΔC_p) on binding of the two metal ions.[13] In this case the LFSE model is an oversimplification.

Why is the preference of the Zn finger for zinc driven by enthalpy without EEC whereas that of CAII is driven by entropy with complex compensation? We propose that the structural metal ion binding site of a Zn finger—completely encaged by the peptide minidomain—provides an example of a *sealed* site whereas the catalytic metal ion binding site of CAII exemplifies an *exposed* site, coupled to its environment via a solvent-derived ligand. This perspective suggests that selectivity of a sealed site for Zn^{2+} (relative to Co^{2+}) would be governed by LFSE (*9*) and Williams−Irving terms (*31*) due to decoupling of its d orbitals from the environment; selectivity of an exposed site would be enforced by ECC. The limitations of the LFSE model thus honor in the breach the importance of environmental coupling in the mechanism of thermodynamic compensation. We propose that ITC experiments may be of general value to distinguish between these classes of metal-binding sites: limited compensation may provide a general signature of a sealed Zn^{2+}-binding site.

CONCLUDING REMARKS

LFSE provides an integral but incomplete contribution to the metal ion selectivity of zinc metalloproteins. For closed sites as observed in Zn or Co fingers, intrinsic differences in electron affinities and subtle distortions in ideal tetrahedral geometry (collectively designated Irving−Williams terms) are likely to contribute to both overall zinc affinities and the lower stabilities of corresponding cobalt complexes. Whereas such terms may or may not incur entropic compensation, LFSE is formally without EEC. The limited thermodynamic compensation observed in calorimetric studies of CP-1 and WT1-p thus suggests that LFSE plays a major (and perhaps even predominant) role in determining the ratio of Zn to Co affinities. For open sites as observed in CAII and other zinc metalloenzymes, the complex interplay of structural adjustment in the protein and changes in solvent reorganization leads to significant EEC. Neither LFSE nor metal-specific enthalpies of hydration (which are subsumed within the LFSE thermodynamic cycle) are predominant.

CP-1 and WT1-p exhibit homologous structures but different Zn:Co binding ratios: higher (CPI-1) or lower (WT-1p) than is predicted by LFSE on the basis of model compounds. The large variation observed in the stringency of metal ion selectivity among Zn fingers poses a significant challenge to physical understanding. We suggest that a general theoretical framework will be provided by the energy landscape picture of protein folding. Coupling between subtle changes in the metal ion binding site (imposed by Irving−Williams terms) and the surrounding peptide matrix is proposed to modulate the enthalpic advantage of Zn binding. This view implies that the formal absence of EEC characteristic of LFSE is only approximate and may be violated at the extremes of high or low Zn:Co binding ratios. In the future it would be of interest to investigate whether a correlation between the rigidity of the Zn finger and the stringency of its metal ion selectivity (as suggested by comparison of CP-1 and WT1-p) will generally be observed.

ACKNOWLEDGMENT

M.A.W. is deeply grateful to R. J. P. Williams (University of Oxford) for discussion and encouragement. We thank Prof. J. Sturtevant (Yale University) for advice and access to a calorimeter in the early stages of this work, C. E. Dahl for peptide synthesis, N. Phillips for assistance with peptide purification, and Professors V. Anderson (Case Western Reserve University), B. Bosnich (University of Chicago), J. Karn (Case Western Reserve University), H. Qian (University of Washington), and D. Wilcox (Dartmouth College) for helpful discussion.

SUPPORTING INFORMATION AVAILABLE

Seven figures providing thermodynamic data for EDTA derivatives, 1D and 2D NMR spectra of WT1-p, a summary of sequential assignment in Wüthrich format, a Ramachandran plot, RMS difference (RMSD) values relative to the crystal structure of the homologous Zif268 finger, Raman deconvolution, and a model of the T22 hydrogen bond and five tables providing chemical shifts, information regarding the minor conformational substate of the finger, and distance geometry (DG)/restrained molecular dynamics (RMD) restraints. This material is available free of charge via the Internet at http://pubs.acs.org.

REFERENCES

1. Maret, W., and Vallee, B. L. (1993) Cobalt as probe and label of proteins, *Methods Enzymol. 226*, 52−71.

[13] A negative change in heat capacity was observed on binding of Zn^{2+} (but not Co^{2+}) to CAII. This was ascribed to (a) more efficient desolvation of nonpolar protein surfaces in the active-site cleft, (b) more efficient shielding of Zn^{2+} than Co^{2+} in the protein complex, or (c) intrinsic differences between Zn^{2+} and Co^2 in the ΔC_p of hydration. None of these possibilities seem satisfactory as crystal structures of Zn^{2+}- and Co^{2+}-CAII complexes are essentially identical, suggesting similar extents of desolvation and shielding in the active site (*54*, *68*). Standard values of ΔC_p of hydration of Zn^{2+} and Co^{2+} are also similar (*81*).

2. Klug, A., and Rhodes, D. (1987) Zinc fingers a novel protein motif for nucleic acid recognition, *Trends Biochem. Sci. 12*, 464−469.
3. Pavletich, N. P., and Pabo, C. O. (1991) Zinc finger-DNA recognition: crystal structure of a Zif268-DNA complex at 2.1 Å, *Science 252*, 809−817.
4. Luisi, B. F., Xu, W., Otwinowski, Z., Freedman, L. P., Yamamoto, K. R., and Sigler, P. B. (1991) Crystallographic analysis of the interaction of the glucocorticoid receptor with DNA, *Nature 352*, 497−505.
5. Berg, J. M., and Shi, Y. (1996) The galvanization of biology: a growing appreciation of the role of zinc, *Science 271*, 1081−1085.
6. Frankel, A. D., Berg, J. M., and Pabo, C. O. (1987) Metal-dependent folding of a single zinc finger from transcription factor IIIA, *Proc. Natl. Acad. Sci. U.S.A. 84*, 4841−4845.
7. Parraga, G., Horvath, S. J., Eisen, A., Taylor, W. E., Hood, L., Young, E. T., and Klevit, R. E. (1988) Zinc-dependent structure of a single-finger domain of yeast ADR1, *Science 241*, 1489−1492.
8. Lee, M. S., Gippert, G. P., Soman, K. V., Case, D. A., and Wright, P. E. (1989) Three-dimensional solution structure of a single zinc finger DNA-binding domain, *Science 245*, 635−637.
9. Berg, J. M., and Merkle, D. L. (1989) On the metal ion specificity of "Zn finger" proteins, *J. Am. Chem. Soc. 111*, 3779−3781.
10. Fraústro da Silva, J. J. R., and Williams, R. J. P. (2001) *The biological chemistry of the elements. The inorganic chemistry of life*, 2nd ed., Oxford University Press, Oxford.
11. Lippard, S. J., and Berg, J. M. (1994) *Principles of Bioinorganic Chemistry*, University Science Books, Mill Valley, CA.
12. Call, K. M., Glaser, T., Ito, C. Y., Buckler, A. J., Pelletier, J., Haber, D. A., Rose, E. A., Kral, A., Yeger, H., Lewis, W. H., Jones, C., and Houseman, D. E. (1990) Isolation and characterization of a zinc finger polypeptide gene at the human chromsome 11 Wilms' tumor locus, *Cell 60*, 509−520.
13. Bruening, W., Bardeesy, N., Silverman, B. L., Cohn, R. A., Machin, G. A., Aronson, A. J., Houseman, D., and Pelletier, J. (1992) Germline intronic and exonic mutations in the Wilms' tumour gene (WT1) affecting urogenital development, *Nat. Genet. 1*, 144−148.
14. Blasie, C. A., and Berg, J. M. (2002) Structure-based thermodynamic analysis of a coupled metal binding-protein folding reaction involving a zinc finger peptide, *Biochemistry 41*, 15068−15073.
15. Danil de Namor, A. F. (1988) Linear correlation between entropies of complexation of cryptand 222 with metal ions in non-aqueous solvents and entropies of solvation of these ions in these solvents, *J. Chem. Soc., Faraday Trans. 1 84*, 2441−2444.
16. DiTusa, C. A., McCall, K. A., Christensen, T., Mahapatro, M., Fierke, C. A., and Toone, E. J. (2001) Thermodynamics of metal ion binding. 2. Metal ion binding by carbonic anhydrase variants, *Biochemistry 40*, 5345−5351.
17. DiTusa, C. A., Christensen, T., McCall, K. A., Fierke, C. A., and Toone, E. J. (2001) Thermodynamics of metal ion binding. 1. Metal ion binding by wild-type carbonic anhydrase, *Biochemistry 40*, 5338−5344.
18. Christensen, T., Gooden, D. M., Kung, J. E., and Toone, E. J. (2003) Additivity and the physical basis of multivalency effects: a thermodynamic investigation of the calcium EDTA interaction, *J. Am. Chem. Soc. 125*, 7357−7366.
19. Sharp, K. (2001) Entropy-enthalpy compensation: fact or artifact? *Protein Sci. 10*, 661−667.
20. Liu, L., and Guo, Q. X. (2001) Isokinetic relationship, isoequilibrium relationship, and enthalpy-entropy compensation, *Chem. Rev. 101*, 673−695.
21. Dunitz, J. D. (1995) Win some, lose some: enthalpy-entropy compensation in weak intermolecular interactions, *Chem. Biol. 2*, 709−712.
22. Searle, M. S., Westwell, M. S., and Williams, D. H. (1995) Application of a generalised enthalpy-entropy relationship to binding co-operativity and weak associations in solution, *J. Chem. Soc., Perkin Trans. 2*, 141−151.
23. Lumry, R., and Rajender, S. (1970) Enthalpy-entropy compensation phenomena in water solutions of proteins and small molecules: a ubiquitous property of water, *Biopolymers 9*, 1125−1227.
24. Grunwald, E., and Steel, C. (1995) Solvent reorganization and thermodynamic enthalpy-entropy compensation, *J. Am. Chem. Soc. 117*, 5687−5692.
25. Lachenmann, M. J., Ladbury, J. E., Phillips, N. B., Narayana, N., Qian, X., and Weiss, M. A. (2002) The hidden thermodynamics of a zinc finger, *J. Mol. Biol. 316*, 969−989.
26. Lachenmann, M. J., Ladbury, J. E., Qian, X., Huang, K., Singh, R., and Weiss, M. A. (2004) The hidden thermodynamics of a zinc finger probed by non-standard repair of a protein crevice, *Protein Sci.* (in press).
27. Lindskog, S., and Nyman, P. O. (1964) Metal-binding properties of human erythrocyte carbonic anhydrase, *Biochim. Biophys. Acta 85*, 462−474.
28. Discenza, M. T., and Pelletier, J. (2004) Insights into the physiological role of WT1 from studies of genetically modified mice, *Physiol. Genomics 16*, 287−300.
29. Oschkinat, H., Cieslar, C., Gronenborn, A. M., and Clore, G. M. (1989) Three-dimensional homonuclear Hartmann-Hahn-nuclear Overhauser enhancement spectroscopy in H_2O and its applications to proteins, *J. Magn. Reson. 81*, 212−216.
30. Dong, J., Wan, Z., Popov, M., Carey, P. R., and Weiss, M. A. (2003) Insulin assembly damps conformational fluctuations: Raman analysis of amide I line widths in native states and fibrils, *J. Mol. Biol. 330*, 431−442.
31. Irving, H., and Willimas, R. J. P. (1953) The stability of transition-metal complexes, *J. Chem. Soc.* 3192−3210.
32. Onuchic, J. N., Luthey-Schulten, Z., and Wolynes, P. G. (1997) Theory of protein folding: the energy landscape perspective, *Annu. Rev. Phys. Chem. 48*, 545−600.
33. Pande, V. S., Grosberg, A., Tanaka, T., and Rokhsar, D. S. (1998) Pathways for protein folding: is a new view needed? *Curr. Opin. Struct. Biol. 8*, 68−79.
34. Lazaridis, T., and Karplus, M. (2003) Thermodynamics of protein folding: a microscopic view, *Biophys. Chem. 100*, 367−395.
35. Merrifield, B. (1986) Solid phase synthesis, *Science 232*, 341−347.
36. Wiseman, T., Williston, S., Brandts, J. F., and Lin, L. N. (1989) Rapid measurement of binding constants and heats of binding using a new titration calorimeter, *Anal. Biochem. 179*, 131−137.
37. Ladbury, J. E., and Chowdhry, B. Z. (1996) Sensing the heat: the application of isothermal titration calorimetry to thermodynamic studies of biomolecular interactions, *Chem. Biol. 3*, 791−801.
38. Dong, J., Dinankarpandian, D., and Carey, P. R. (1998) Extending the Raman analysis of biological samples to the 100 micromolar concentration cange, *Appl. Spectrosc. 52*, 1117−1122.
39. Kochoyan, M., Havel, T. F., Nguyen, D. T., Dahl, C. E., Keutmann, H. T., and Weiss, M. A. (1991) Alternating zinc fingers in the human male associated protein ZFY: 2D NMR structure of an even finger and implications for "jumping-linker" DNA recognition, *Biochemistry 30*, 3371−3386.
40. Smallcombe, S. H. (1993) Solvent suppression with symmetrically-shifted pulses, *J. Am. Chem. Soc. 115*, 4776−4785.
41. Laskowski, R. A. (1995) SURFNET: a program for visualizing molecular surfaces, cavities and intermolecular interactions, *J. Mol. Graphics 13*, 323−330.
42. Lee, B., and Richards, F. M. (1971) The interpretation of protein structure: estimation of static accessibility, *J. Mol. Biol. 55*, 379−400.
43. Lee, J. D. (1991) *Concise Inorganic Chemistry*, 4th ed., Chapman & Hall, London.
44. Schubert, J., Lind, E. L., Westfall, W. M., Pfleger, R., and Li, N. C. (1958) Ion-exchange and solvent-extraction studies on Co(II) and Zn(II) complexes of soem organic acids, *J. Am. Chem. Soc. 80*, 4799−4802.
45. Li, N. C., and Manning, R. A. (1955) Some metal complexes of sulfur-containing amino acids, *J. Am. Chem. Soc. 77*, 5225−5227.
46. Martell, A. E. (1964) *Stability Constants of Metal-Ion Complexes*, The Chemical Society, London.
47. Silber, H. B., and Murguia, M. A. (1985) Spectrophotometric investigations of the ocathedral-tetrahedral equilibria in cobalt-(II)-thiocynate systems in aqueous methanol, *Inorg. Chem. 24*, 3794−3802.
48. Laity, J. H., Dyson, H. J., and Wright, P. E. (2000) Molecular basis for modulation of biological function by alternate splicing of the Wilms' tumor suppressor protein, *Proc. Natl. Acad. Sci. U.S.A. 97*, 11932−11935.
49. Harper, L. V., Amann, B. T., Vinson, V. K., and Berg, J. M. (1993) NMR studies of a cobalt-substituted zinc finger peptide, *J. Am. Chem. Soc. 115*, 2577−2580.
50. Qian, X., and Weiss, M. A. (1992) Two-dimensional NMR studies of the zinc finger motif: solution structures and dynamics of mutant ZFY domains containing aromatic substitutions in the hydrophobic core, *Biochemistry 31*, 7463−7476.

51. Narayan, V. A., Kriwacki, R. W., and Caradonna, J. P. (1997) Structures of zinc finger domains from transcription factor Sp1. Insights into sequence-specific protein-DNA recognition, *J. Biol. Chem. 272*, 7801−7809.
52. Miura, T., Satoh, T., and Takeuchi, H. (1998) Role of metal-ligand coordination in the folding pathway of zinc finger peptides, *Biochim. Biophys. Acta 1384*, 171−179.
53. Pavletich, N. P., and Pabo, C. O. (1993) Crystal structure of a five-finger GLI-DNA complex: new perspectives on zinc fingers, *Science 261*, 1701−1707.
54. Eriksson, A. E., Jones, T. A., and Liljas, A. (1988) Refined structure of human carbonic anhydrase II at 2.0 Å resolution, *Proteins: Struct., Funct., Genet. 4*, 274−282.
55. Gomez, J., and Freire, E. (1995) Thermodynamic mapping of the inhibitor site of the aspartic protease endothiapepsin, *J. Mol. Biol. 252*, 337−350.
56. Schwarzenbach, G. (1952) Der Chelateffekt, *Helv. Chim. Acta 35*, 2344−2359.
57. Williams, R. J. P. (1954) The stability of complex ions with special reference to hydration, *J. Phys. Chem. 58*, 121−126.
58. Hanas, J. S., Hazuda, D. J., Bogenhagen, D. F., Wu, F. Y., and Wu, C. W. (1983) Xenopus transcription factor A requires zinc for binding to the 5 S RNA gene, *J. Biol. Chem. 258*, 14120−14125.
59. Berg, J. M. (1988) Proposed structure for the zinc-binding domains from transcription factor TFIIIA and related proteins, *Proc. Natl. Acad. Sci. U.S.A. 85*, 99−102.
60. Rees, D. C. (2002) Great metalloclusters in enzymology, *Annu. Rev. Biochem. 71*, 221−246.
61. Berkner, I. V., and Marshall, L. C. (1965) On the origin and rise of oxygen concentration in the earth's atmosphere, *J. Atmos.. Sci. 22*, 225−261.
62. Canfield, D. E., Habicht, K. S., and Thamdrup, B. (2000) The Archean sulfur cycle and the early history of atmospheric oxygen, *Science 288*, 658−661.
63. Eschenmoser, A. (1994) B_{12}: reminiscences and after-thoughts, *Ciba Found. Symp. 180*, 309−329.
64. Anbar, A. D., and Knoll, A. H. (2002) Proterozoic ocean chemistry and evolution: a bioinorganic bridge? *Science 297*, 1137−1142.
65. Liljas, A., Kannan, K. K., Bergsten, P.-C., Waara, I., Fridborg, K., Strandberg, B., Carlbom, U., Jarup, L., Lovgren, S., and Petef, M. (1972) Crystal structure of human carbonic anhydrase C, *Nat. New Biol. 235*, 131−137.
66. Forsman, C., Behravan, G., Osterman, A., and Jonsson, B. H. (1988) Production of active human carbonic anhydrase II in *E. coli*, *Acta Chem. Scand., B 42*, 314−318.
67. Hakansson, K., Carlsson, M., Svensson, L. A., and Liljas, A. (1992) Structure of native and apo carbonic anhydrase II and structure of some of its anion-ligand complexes, *J. Mol. Biol. 227*, 1192−1204.
68. Hakansson, K., and Wehnert, A. (1992) Structure of cobalt carbonic anhydrase complexed with bicarbonate, *J. Mol. Biol. 228*, 1212−1218.
69. Blundell, T. L., Cutfield, J. F., Cutfield, S. M., Dodson, E. J., Dodson, G. G., Hodgkin, D. C., Mercola, D. A., and Vijayan, M. (1971) Atomic positions in rhombohedral 2-zinc insulin crystals, *Nature 231*, 506−511.
70. Smith, G. D., Pangborn, W. A., and Blessing, R. H. (2001) Phase changes in T_3R_{3f} human insulin: temperature or pressure induced? *Acta Crystallogr. D57*, 1091−1100.
71. McGraw, S. E., and Lindenbaum, S. (1990) The use of microcalorimetry to measure thermodynamic parameters of the binding of ligands to insulin, *Pharm. Res. 7*, 606−611.
72. Kuroki, R., Nitta, K., and Yutani, K. (1992) Thermodynamic changes in the binding of Ca^{2+} to a mutant human lysozyme (D86/92). Enthalpy-entropy compensation observed upon Ca^{2+} binding to proteins, *J. Biol. Chem. 267*, 24297−24301.
73. Searle, M. S., and Williams, D. H. (1992) The cost of conformational order: entropy changes in molecular associations, *J. Am. Chem. Soc. 114*, 10690−10697.
74. Yang, D., Mok, Y. K., Forman-Kay, J. D., Farrow, N. A., and Kay, L. E. (1997) Contributions to protein entropy and heat capacity from bond vector motions measured by NMR spin relaxation, *J. Mol. Biol. 272*, 790−804.
75. Gallicchio, E., Kubo, M. M., and Levy, R. M. (1998) Entropy-enthalpy compensation in solvation and ligand binding revisited, *J. Am. Chem. Soc. 120*, 4526−4527.
76. Yu, H.-A., and Karplus, M. (1988) A thermodynamic analysis of solvation, *J. Chem. Phys. 89*, 2366−2379.
77. Chervenak, M., and Toone, E. J. (1994) A direct measure of the contribution of solvent reorganization to the enthalpy of ligand binding, *J. Am. Chem. Soc. 116*, 10534−10539.
78. Eftink, M. R., Anusiem, A. C., and Biltonen, R. T. (1983) Enthalpy-entropy compensation and heat capacity changes for protein-ligand interactions: general thermodynamic models and data for the binding of nucleotides to ribonuclease A, *Biochemistry 22*, 3884−3896.
79. Qian, H., and Hopfield, J. J. (1996) Entropy-enthalpy compensation: perturbation and relaxation in thermodynamic systems, *J. Chem. Phys. 105*, 9292−9298.
80. Qian, H. (1998) Entropy-enthalpy compensation: conformational fluctuation and induced-fit, *J. Chem. Phys. 109*, 10015−10017.
81. Marcus, Y. (1994) A simple empirical model describing the thermodynamics of hydration of ions of widely varying charges, sizes, and shapes, *Biophys. Chem. 51*, 111−127.
82. Krizek, B. A., Merkle, D. L., and Berg, J. M. (1993) Ligand variation and metal-ion binding specificity in zinc finger peptides, *Inorg. Chem. 32*, 937−940.
83. Green, L. M., and Berg, J. M. (1989) A retroviral Cys-Xaa_2-Cys-Xaa_4-Hiss-Xaa_4-Cys peptide binds metal ions: spectroscopic studies and a proposed three-dimensional structure, *Proc. Natl. Acad. Sci. U.S.A. 86*, 4047−4051.
84. Magyar, J. S., and Godwin, H. A. (2003) Spectropotentiometric analysis of metal binding to structural zinc-binding sites: accounting quantitatively for pH and metal ion buffering effects, *Anal. Biochem. 320*, 39−54.
85. Payne, J. C., Rous, B. W., Tenderholt, A. L., and Godwin, H. A. (2003) Spectroscopic Determination of the Binding Affinity of Zinc to the DNA-Binding Domains of Nuclear Hormone Receptors, *Biochemistry 42*, 14214−14224.
86. McLendon, G., Hull, H., Larkin, K., and Chang, W. (1999) Metal binding to the HIV nucleocapsid peptide, *J. Biol. Inorg. Chem. 4*, 171−174.
87. Berkovits, H. J., and Berg, J. M. (1999) Metal and DNA binding properties of a two-domain fragment of neural zinc finger factor 1, a CCHC-type zinc binding protein, *Biochemistry 38*, 16826−16830.
88. Maiti, N. C., Apetri, M. M., Zagorski, M. G., Carey, P. R., and Anderson, V. E. (2004) Spectroscopic characterization of secondary structure in natively unfolded proteins: alpha-synuclein, *J. Am. Chem. Soc. 126*, 2399−2408.
89. Sane, S. U., Cramer, S. M., and Przybycien, T. M. (1999) A holistic approach to protein secondary structure characterization using amide I band Raman spectroscopy, *Anal. Biochem. 269*, 255−272.
90. Peticolas, W. L. (1995) Raman spectroscopy of DNA and proteins, *Methods Enzymol. 246*, 389−416.
91. Berjot, M., Marx, J., and Alix, A. J. P. (1987) Determination of the secondary structure of proteins from the Raman amide I band: the reference intensity profile method, *J. Raman Spectrosc. 18*, 289−300.
92. Krizek, B. A., Zawadzke, L. E., and Berg, J. M. (1993) Independence of metal binding between tandme Cys2His2 zinc finger domains, *Protein Sci. 2*, 1313−1319.
93. Eriksson, A. E., Baase, W. A., and Matthews, B. (1993) Similar hydrophobic replacements of Leu99 amd Phe153 within the core of T4 lysozyme have different structural and thermodynamic consequences, *J. Mol. Biol. 229*, 747−769.
94. Gao, J., Kuczera, K., Tidor, B., and Karplus, M. (1989) Hidden thermodynamics of mutant proteins: a molecular dynamics analysis, *Science 244*, 1069−1072.
95. Corwin, D. T. J., Gruff, E. S., and Koch, S. A. (1987) Zinc, cobalt, and cadmium thiolate complexes: models for the Zinc(S-cys)$_2$-(his)$_2$ centre in transcription factor IIIA (cys=cysteine; his=histidine), *J. Chem. Soc., Chem. Commun.* 966−967.
96. Tripp, B. C., Bell, C. B. r., Cruz, F., Krebs, C., and Ferry, J. G. (2004) A role for iron in an ancient carbonic anhydrase, *J. Biol. Chem. 279*, 6683−6687.
97. Atkins, P. W. (1990) *Physical Chemistry*, 4th ed., Oxford University Press, Oxford.
98. Derewenda, U., Derewenda, Z., Dodson, E. J., Dodson, G. G., Reynolds, C. D., Smith, G. D., Sparks, C., and Swenson, D. (1989) Phenol stabilizes more helix in a new symmetrical zinc insulin hexamer, *Nature 338*, 594−596.

BI0491999